

Mass Spectrometric Fingerprints of Organic Compounds in NaCl-Rich Ice Grains from Europa and Enceladus

Maryse Napoleoni¹, Fabian Klenner¹, Nozair Khawaja¹, Jon K. Hillier¹, Frank Postberg¹*

¹Institute of Geological Sciences, Freie Universität Berlin, Berlin 12249, Germany

*corresponding author: m.napoleoni@fu-berlin.de

ABSTRACT

Europa and Enceladus, respective moons of Jupiter and Saturn, are prime targets in the exploration of potentially habitable extraterrestrial ocean worlds. Organic material could be incorporated from the ocean into ice grains ejected from the surface or in potential plumes and detected via spacecraft flybys with impact ionization mass spectrometers, such as the SURface Dust Analyzer (SUDA) onboard Europa Clipper or the Cosmic Dust Analyzer (CDA) onboard the past Cassini mission. Ice grains ejected from both Europa and Enceladus are expected to contain sodium salts, specifically sodium chloride (NaCl), in varying concentrations. Consequently, it is important to understand its effects on the mass spectrometric signatures of organic material in salt-rich ice grains. Previous studies have only focused on the detection of biosignatures, such as amino acids, in salt-rich ice grains. We here perform analogue experiments using the Laser Induced Liquid Beam Ion Desorption (LILBID) technique to study how a wide variety of abiotic and potentially biotic organic molecules could be identified by

SUDA-type instruments. We investigate their mass spectral characteristics and detectability at various typical NaCl-concentrations expected for salt-rich ice grains and in both cation and anion mode. Results show that organics in salt-rich ice grains can still be detected because of the formation of molecular ions and sodiated and chlorinated species. However, high salt concentrations induce compound- and concentration-dependent suppression effects, depending on the chemical properties and functional groups of the analytes. Our results emphasize the need of both ion modes to detect a wide range of organics embedded in complex matrices, and to discriminate between abiotic and potentially biotic species. This work complements a spectral reference library for Europa Clipper and other ocean world missions.

KEYWORDS

Ocean worlds, Europa Clipper, SUDA, Analogue experiments, Mass spectrometry, LILBID, salt matrix effects, ice grains

1 Introduction

Ocean worlds are of growing interest for life detection missions. In particular, Jupiter's moon Europa and Saturn's moon Enceladus both have a high potential to host extant biological life in their global subsurface water oceans¹⁻⁴ with uniquely hospitable chemistry⁵. Europa's ocean is thought to be in contact on its lower part with a rocky silicate seafloor, and on its upper part with an ice shell that may have tectonic activity allowing reductant-oxidant cycling^{6,7}; and it might have been present for much of the history of the solar system, providing a long-term stable environment with geochemical interactions, essential elements, and energy sources for an independent origin of life⁸⁻¹¹. Enceladus's subsurface ocean of salty water^{12, 13} is also thought to be long lived and hosts a variety of organic material, including compounds made of the biologically essential elements carbon, hydrogen, oxygen, nitrogen, and phosphorus¹⁴⁻¹⁷ potentially acting as building blocks or byproducts of life. The discovery of hydrothermal processes at the interface between the ocean and the rocky core of Enceladus was deduced from

the detections of nanometer-scale silica particles ¹⁸ and of molecular hydrogen (H₂)¹⁹, a product of serpentinization reactions, in a large plume of icy particles emanating from cracks in the southern pole ^{20, 21}. These jets of water provide a source of potentially life-bearing material being ejected from the subsurface ocean and emitted to space in icy particles.

Europa's subsurface ocean may be communicating material to the surface through tectonic activity, resurfacing or other forms of upwelling ²², rendering subsurface material analyzable by spacecraft flybys. Organic material possibly related to bioactivity in Europa's subsurface ocean might therefore reach the surface ice and be sputtered to high altitudes by micrometeorite bombardment ^{23, 24} and by energetic heavy ions trapped in Jupiter's magnetosphere ²⁵. Organics could also be incorporated in potential plumes ejecting gas and water ice grains from the subsurface ocean into space ²⁶⁻²⁹. The detection and identification of organics in Enceladus plume ice grains allowed the interpretation of ice grains' origins, their formation mechanisms, and the presence of an organic-rich layer at the upper ocean-ice interface ^{15, 16}. Diverse complex organic species including hydrocarbons, amino acids and carboxylic acids, could be geochemically synthesized in icy moons' oceans by serpentinization reactions and reduction of inorganic precursors³⁰⁻³² in potential hydrothermal systems. Processes such as bubble-scrubbing may increase the concentration of organic material and lead to enriched particles allowing the detection of organic biosignatures in ice grains at a much higher level than expected in the bulk ocean ³³.

Dust analyzers are powerful instruments for the analysis of extraterrestrial ice grains and the identification of molecules therein. A dust analyzer detects individual particles impacting its target at hypervelocities (several km/s), creating an impact plasma whose composition is measured via time-of-flight (TOF) mass spectrometry (MS). Such instruments can detect chemical species embedded in ice at the ppm level, including organic compounds ^{15, 34} and salts

¹², and have revealed some of the most significant advances about the chemistry of the plume of Enceladus ^{35,36}. The Cosmic Dust Analyzer (CDA) onboard the Cassini spacecraft allowed the discovery of complex organic macromolecules with molecular masses above 200 u ¹⁵, as well as smaller reactive nitrogen- and oxygen-bearing molecules ¹⁶ from the ocean of Enceladus. Onboard NASA's upcoming Europa Clipper mission ³⁷, the SURface Dust Analyzer (SUDA) will capture and analyze dust particles released from Europa's surface by impacts and in its potential plumes ³⁸. During close flybys, SUDA will map the composition of encountered ejecta particles onto certain surface features of Europa ^{13,39}. The SUDA instrument is a TOF reflectron-type mass spectrometer optimized for a high mass resolution in the mass range $m=1-500u$. As compared to the CDA instrument that could only detect cations, the SUDA instrument will be able to record both cation and anion mass spectra, aiming to target a wider range of compounds.

The search for organic material and molecular biosignatures in ice grains ejected from ocean worlds with SUDA-type instruments might be challenged by the complex chemistry and salty composition of their ice and oceans. The salinity of Enceladus's ocean is assumed to be roughly similar to Earth's ocean or lower⁴⁰, at around 20 g/kg ⁴¹ and dominated by NaCl at a concentration of 0.05–0.2 mol/kg ¹². At Europa, the strong magnetic induction field measured by Galileo suggested a salinity perhaps in excess of 50 g/kg ⁴². Analysis of the Galileo Near-Infrared Mapping Spectrometer (NIMS) data showed that the Europa's icy surface is dominated by water, sulfuric acid hydrate and other non-ice material. Sulfuric acid hydrate is an expected product of radiolytic chemistry occurring on the heavily irradiated and sulfur-bombarded trailing hemisphere ⁴³⁻⁴⁵. Its detection was confirmed on the trailing hemisphere by telescopic observations, which also detected spatially coincident magnesium sulfate salts, suggesting a radiolytic origin of the sulfate salts ^{46,47}. The non-ice material identified by NIMS has been first interpreted as endogenous sulfate salts originating from the subsurface ocean ⁴⁸⁻

⁵¹. Ground-based spectroscopic observations have proposed sodium chloride and potassium chloride⁴⁶ or a mixture of magnesium chloride, chlorate, and perchlorate⁵² as the dominant non-ice component of the leading hemisphere. The non-ice material is likely a combination of multiple materials, including frozen brines, sulfate salts and chlorides or chlorates, with relative proportions varying spatially over Europa's leading and trailing hemispheres. Endogenous material reflecting the composition of the interior ocean is thought to be particularly abundant in the chaos terrains of the leading hemisphere, as these terrains are geologically young, are potential regions of subsurface upwelling or melt-through ^{53, 54} and are shielded from the sulfur ion implantation of the trailing hemisphere. Chaos terrains are rich in sodium chloride ^{47, 55-57}, an inorganic salt likely to be a major component of Europa's ocean, as this salt is expected to dominate in an ocean with an extensive hydrothermal circulation ⁵⁸. Sodium chloride is estimated to be present at a mean concentration of 0.1-1.2 mol/kg H₂O ⁷, but surface ice inhomogeneities could even increase the salt concentrations, leading the Europa lander mission concept to request that onboard instruments should be prepared for samples containing up to 30% salt ⁵⁹. Analytical instruments aiming at investigating the chemical composition and possible biosignature content of ocean worlds will therefore have to deal with native samples containing significant amounts of salts.

Interpreting mass spectra acquired in space from SUDA-type instruments requires terrestrial calibration by analogue experiments. Spaceborne impact ionization mass spectrometers analyze projectile ions from ice grains impacting onto metal targets. It is challenging to recreate this impact process in laboratories, because micrometer-sized ice grains cannot currently be easily accelerated at relevant speeds ^{60, 61}. Therefore, the Laser Induced Liquid Beam Ion Desorption (LILBID) technique has been developed to simulate the impact ionization mass spectra of ice grains recorded in space at impact speeds from 3 to >20km/s ⁶²⁻⁶⁴ without the need of a dust accelerator. This technique has been used to reproduce compositional differences

of ice grains detected from Enceladus with the CDA instrument^{12, 15, 16}, and to investigate the mass spectral characteristics and fragmentation patterns of organics between different ionization methods⁶⁵. Klenner et al.^{66, 67} used LILBID analogue experiments to investigate the detection of amino acids, fatty acids, and peptides in water-rich and salt-rich ice grains in an ocean world scenario, as they could be identified by future spaceborne mass spectrometers such as SUDA or the Enceladus Ice Analyzer (ENIA)⁶⁸. They found that these bioessential compounds can be detected down to the micro- or nanomolar level, with optimal encounter velocities of 4-6 km/s, and that these complex organic molecules remained largely intact up to encounter velocities of 8 km/s. Moreover, characteristic abiotic and biotic fingerprints could be discriminated in the mass spectra. Recently, the investigation of bacterial extracts showed that microbial biosignatures could be reliably identified at the ppm level in salt-rich ice grains, and that the sensitivity to biosignatures decreases with increasing salt concentration⁶⁹.

In impact ionization mass spectrometry, the matrix from which a sample is analyzed can increase or decrease the ionization process, hence influencing ion formation and the resulting spectra^{70, 71}. In particular, salts in the analyte solution can cause a significant degradation of the signal-to-noise ratio and lead to ion suppression and adduct formation, which may mask or complicate the ion signals with interferences. Matrix effects can therefore limit the quantitative and qualitative analysis of SUDA-type instruments, which are likely to analyze salty and oxidant-rich ice grains reflecting icy moons' compositions. To prevent these difficulties, laboratory analogue experiments investigating salt-rich matrices are required. A previous study by Klenner et al.⁶⁷ investigated the spectral appearance of amino acids in salt-rich solutions. They found that, although high salt concentrations suppress characteristic organic peaks, amino acids typically form sodiated (sodium-complexed) molecules in which a sodium ion replaces a hydrogen ion and could be detected down to micromolar concentrations.

This work investigates the characteristic mass spectral signatures of several water-soluble organics in salt-rich ice grains reflecting the composition of Europa and Enceladus. We discuss data collected from LILBID analogue experiments in which we examine the effects of sodium chloride (NaCl), at concentrations of 0.01, 0.1 and 1M NaCl, on the spectral appearance of organic molecules and their detectability with SUDA-type instruments. We focus on the mass spectral signatures of 5-amino-1-pentanol, acetic acid, benzoic acid, butylamine, glucose, methanol, and pyridine, in both cation and anion mode, to infer general rules predicting the behavior of organic species containing a wide range of functional groups, namely hydroxyl, azine, (aromatic) carboxylic acid, (aromatic) amine, and alkanolamine. Such functional groups are especially relevant for icy moons, because oxygen- and nitrogen-bearing as well as aromatics compounds have been detected on Enceladus ice grains^{15, 16}. Sugars and N-heterocycles are especially relevant for astrobiology investigations as they are essential to biological processes in all terrestrial life and may have played an important role in the origin and evolution of life^{72, 73, 74}. The purpose of this study is to form a better understanding of peak suppression and matrix effects involving salts and different organic species as if detected in icy moons' ice grains by impact ionization mass spectrometers.

2 Experimental Section

2.1 Laser Induced Liquid Beam Ion Desorption (LILBID) Experimental Setup

The experimental LILBID setup (Figure 1) was used to record mass spectra of several solutions of organic compounds in salt-rich water matrices. It has been described in detail by Klenner et al.⁶⁴.

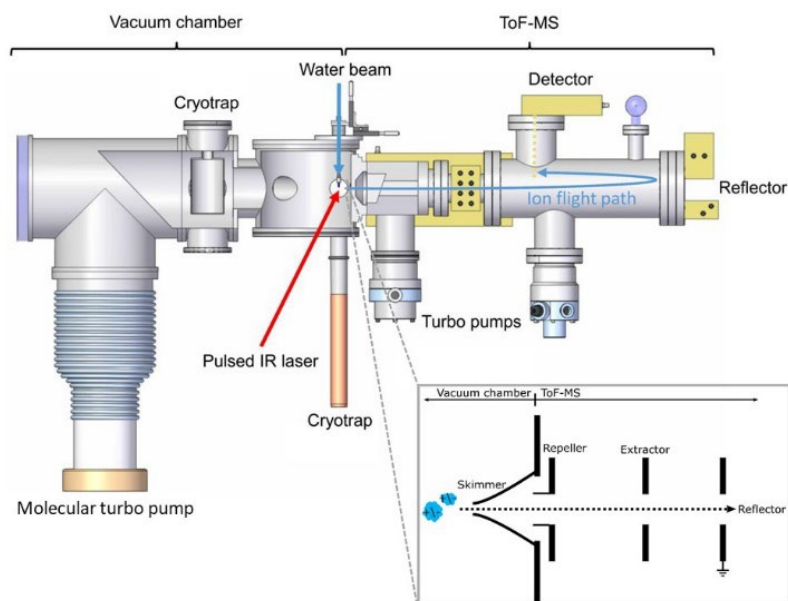



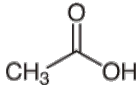
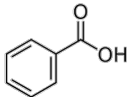

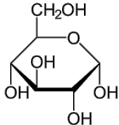

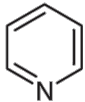
Figure 1. The Laser Induced Liquid Beam Ion Desorption (LILBID) laboratory setup, reproducing the impact ionization mass spectra of ice grains recorded in space (figure reproduced from Klenner et al. (2019)⁶⁴. Copyright [2019] *Rapid Communications in Mass Spectrometry*, Wiley). The principle of delayed extraction of the ions as a function of their initial velocities is shown on the bottom right insert.

The LILBID setup comprises a vacuum chamber, where the sample is ionized, and a time-of-flight mass spectrometer, which detects and analyzes the created ions. In the vacuum chamber, the impact ionization process is simulated by irradiating a micrometer-sized liquid water beam and dissolved substances therein with a pulsed (20 Hz, 7 ns pulse length) infrared laser ($\lambda=2840$ nm) at variable laser energies (up to 4 mJ). The laser energy is absorbed by the water molecules, creates a thermal explosion, and breaks the analyte solution into charged and uncharged atomic, molecular and macroscopic fragments^{75, 76}. After passing through a field-free drift region, the created ions (cations or anions, depending on the chosen polarity) are then accelerated and analyzed in the TOF mass spectrometer with a mass resolution of 600-800 $m/\Delta m$. The principle of delayed extraction allows ions to be selected for analyses as a function of their initial velocities (see Supporting Information, Additional Methods). By adjusting the

delay time together with the laser's power density, different impact speeds of ice grains onto the space instrument's metal target can be accurately simulated ⁶⁴. Both impact ionization and the laser desorption experiment almost exclusively produce singly-charged ions. Ion signals are amplified, digitized (Analog-to-Digital converter) and recorded with a LabVIEW-controlled computer. Each mass spectrum presented here is the average of 300 individual, co-added spectra. The recorded spectra are stored in a newly developed database containing analogue data for impact ionization mass spectrometers, available at <https://lilbid-db.planet.fu-berlin.de> ⁷⁷.

2.2 Organic Solutions

Seven organic species containing a wide range of functional groups, namely hydroxyl, azine, (aromatic) carboxylic acid, (aromatic) amine, and alkanolamine, were investigated (Table 1): 5-amino-1-pentanol (C₅H₁₃NO), acetic acid (C₂H₄O₂), benzoic acid (C₇H₆O₂), butylamine (C₄H₁₁N), glucose (C₆H₁₂O₆), methanol (CH₄O), and pyridine (C₅H₅N). Each compound was dissolved in distilled, deionized Milli-Q purified water and NaCl-rich solutions at a concentration of 5wt% of the organic species, except for benzoic acid that was dissolved at a concentration of 0.17wt% due to its low solubility in water. Each organic compound was measured in pure water and in three solutions of different NaCl concentration (0.01M, 0.1M and 1M NaCl) with the LILBID setup. Because of the low purity of the glucose sample, the Na ion exchange resin amberlite was added to the "pure water" glucose solution to record cation mode spectra. The LILBID setup was checked for contamination and cleaned between sample measurements.

	5-amino-1-pentanol 	Acetic acid 	Benzoic acid 	Butylamine 	Glucose 	Methanol 	Pyridine 
--	---	--	---	---	--	---	---

Formula	C ₅ H ₁₃ NO	C ₂ H ₄ O ₂	C ₇ H ₆ O ₂	C ₄ H ₁₁ N	C ₆ H ₁₂ O ₆	CH ₄ O	C ₅ H ₅ N	
Molecular weight (u)	103	60	122	73	180	32	79	
pKa	15	4.7	4.2	11	12	15	5	
pH in solution	H ₂ O	12.1	2.4	3.3	12.3	7.1	9.0	8.6
	0.01M NaCl	11.7	2.4	3.0	12.4	7.3	7.1	9.3
	0.1M NaCl	12.0	2.4	2.9	12.3	6.9	6.1	8.4
	1M NaCl	12.0	2.2	2.9	12.1	6.0	5.3	9.3

Table 1. Organic Compounds Investigated in the Experiments, and Their Values of pKa and Measured pH in the Different Solutions Investigated.

3 Results

3.1. NaCl Background Matrix

Several salt ions and clusters were identified in the mass spectra of the NaCl background matrix without any organics. In cation mode, the clusters $[\text{Na}(\text{H}_2\text{O})_n]^+$, $[\text{Na}(\text{NaOH})_n]^+$, $[\text{Na}(\text{NaCl})_n]^+$, $[\text{Na}(\text{NaCl})_n(\text{H}_2\text{O})_m]^+$, $[\text{Na}(\text{NaCl})_n(\text{NaOH})_m]^+$ were identified (Figure 2). These species were also observed by Postberg et al.¹² in analogue LILBID data with pure salt solutions. The spectra with the lowest salt concentration (0.01M NaCl; Figure S1) show a predominance of $[\text{Na}(\text{H}_2\text{O})_n]^+$ clusters, whereas $[\text{Na}(\text{NaCl})_n]^+$ clusters are predominant in 0.1M NaCl and 1M NaCl spectra (Figure 2 and Figure S2). In anion mode, the clusters $[\text{Cl}(\text{H}_2\text{O})_n]^-$, $[\text{Cl}(\text{NaOH})_n]^-$, $[\text{Cl}(\text{NaCl})_n]^-$, $[\text{Cl}(\text{NaCl})_n(\text{H}_2\text{O})_m]^-$, and $[\text{Cl}(\text{NaOH})(\text{NaCl})_n]^-$ were identified (Figure 3). At 0.01M NaCl, $[\text{Cl}(\text{H}_2\text{O})_n]^-$ clusters are predominant (Figure S3), whereas $[\text{Cl}(\text{NaCl})_n]^-$ clusters become predominant at 0.1M and 1M NaCl (Figure 3 and Figure S4). In both ion modes, peaks corresponding to ions containing Cl atom(s) show characteristic ³⁷Cl isotopes.

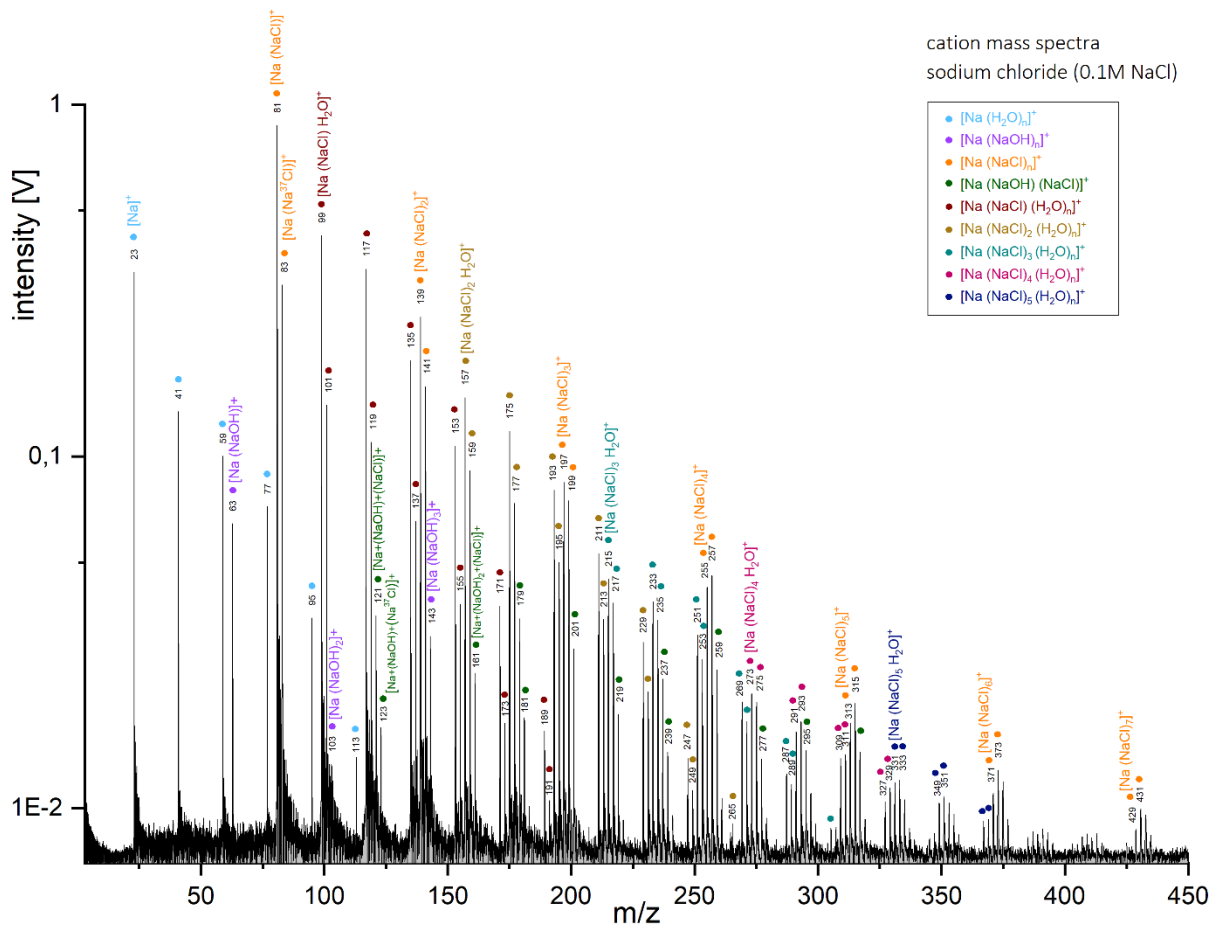


Figure 2. Baseline-corrected cation mass spectrum of sodium chloride (NaCl) at a concentration of 0.1M, recorded at a delay time of 6.1 μ s. Sodiated cations are identified and labeled with their corresponding water clusters.

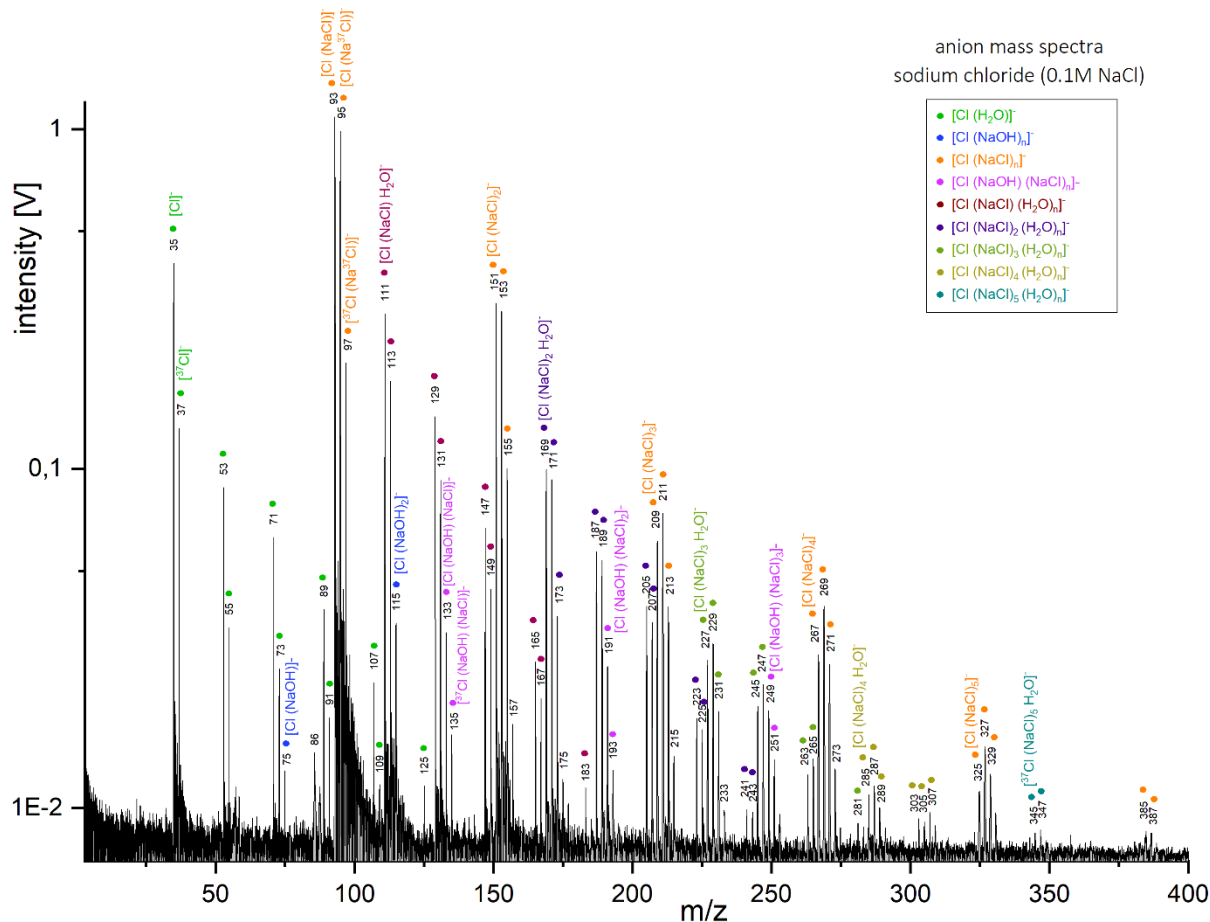


Figure 3. Baseline-corrected anion mass spectrum of sodium chloride (NaCl) at a concentration of 0.1M, recorded at a delay time of 6.1 μ s. Chlorinated anions are identified and labeled with their corresponding water clusters.

3.2 Organic Compounds in Water Matrices

We measured all the organic species in pure water matrices without any salts (Figures S37-S50). We detected protonated molecular peaks ($[M+H]^+$) and deprotonated molecular peaks ($[M-H]^-$) for all organic species, except butylamine, for which no deprotonated molecular peak was observed. We detected prominent $[M-3H]^-$ peaks in the anion spectra of 5-amino-1-pentanol (Figure S38). Positively and negatively charged organic fragments were detected for all compounds except methanol, for which only positively charged fragments were observed (Tables S1 and S2). We detected clusters of the organic species and charged fragments thereof

($[M+M-x]^+$ and $[M+M-x]^-$, with x a fragment of the organic species) or fragmented polymers of the organics (e.g., $[2M-x]^+$ and $[2M-x]^-$, with x a fragment of the organic species) in both cation and anion spectra of 5-amino-1-pentanol (e.g., $[M+(M-OH-NH_3)]^+$; Figures S37 and S38) and pyridine (Figures S49 and S50), in the cation spectra of butylamine (Figure S43) and in the anion spectra of glucose (Figure S46).

3.3 Organic Compounds in NaCl-rich matrices

3.3.1 Low Salt Concentration (0.01M NaCl)

At a concentration of 0.01M NaCl, all the investigated organics form both protonated molecular ions ($[M+H]^+$, with M the molecular mass of the organic compound) and sodiated ions ($[M+Na]^+$) (Table 2), as well as water clusters ($+(H_2O)_n$) of these ions. The intensities of sodiated peaks are usually higher than those of protonated molecular peaks (e.g., Figure 4 and Figures S7, S13, S26 and S31). Positively charged clusters of sodiated organic molecules with NaCl ($[M(NaCl)+Na]^+$) were detected for all organics. Clusters of sodiated organic molecules with NaOH ($[M(NaOH)+Na]^+$) were detected for 5-amino-1-pentanol, butylamine and pyridine, and tentatively detected for both acetic acid and benzoic acid. $[M(NaCl)_n+H]^+$ was detected for benzoic acid and tentatively detected for acetic acid at high delay time (Figures S13 and S8). Disodiated molecules ($[M-H+2Na]^+$) were detected in cation mass spectra of 5-amino-1-pentanol, acetic acid, benzoic acid and glucose, and trisodiated species were detected for glucose ($[M-2H+3Na]^+$) and acetic acid dimers and trimers ($[2M-2H+3Na]^+$, $[3M-2H+3Na]^+$). Clusters of disodiated organic molecules with NaCl ($[M(NaCl)-H+2Na]^+$) were detected only for benzoic acid and acetic acid. Organic fragments were detected for five organics (5-amino-1-pentanol, acetic acid, benzoic acid, butylamine and glucose) in the cation mode (table S1). An adduct of the organic molecule and a charged fragment thereof, $[M+NH_4]^+$, was detected for 5-amino-1-pentanol (Figure 4).

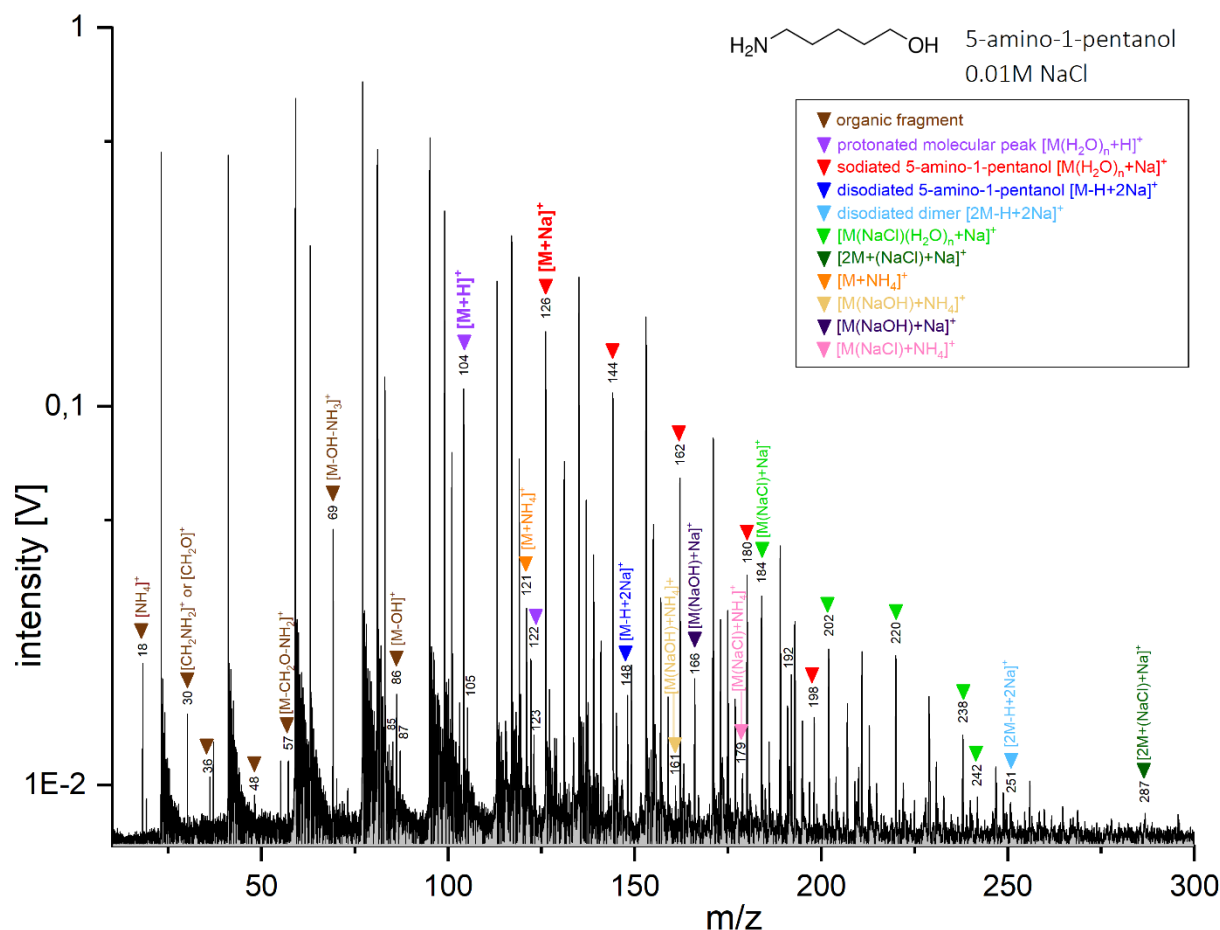


Figure 4. Baseline-corrected cation mass spectrum of 5-amino-1-pentanol at a concentration of 5wt% in a 0.01M NaCl matrix, recorded at a delay time of 6.2 μ s. Unlabeled peaks originate exclusively from the salty matrix.

In anion mode, 5-amino-1-pentanol, acetic acid, benzoic acid and glucose were identified as deprotonated molecular ions ($[M-H]^-$), and 5-amino-1-pentanol, benzoic acid, glucose, methanol and pyridine form chlorinated ions ($[M+Cl]^-$) (Table 3). Salt adducts were detected: $[M(NaCl)_n+Cl]^-$ for 5-amino-1-pentanol and glucose, tentatively for both benzoic acid and methanol; $[M(NaOH)_n+Cl]^-$ tentatively for glucose; $[M(NaCl)_n-H]^-$ for 5-amino-1-pentanol, acetic acid, benzoic acid, and glucose; and $[M(NaOH)-H]^-$ and $[M(NaCl)(NaOH)-H]^-$ for glucose. Dichlorinated anions $[M+H+2Cl]^-$ were tentatively identified for glucose, but this peak interferes with possible $[2M-H-(H_2O)_6]^-$ peaks. Sodiated anion dimers were detected as

$[2M-2H+Na]^-$ for acetic acid, benzoic acid and methanol, and disociated anion oligomers ($[3M-3H+2Na]^-$, $[4M-3H+2Na]^-$) were detected for acetic acid. Negatively charged organic fragments were detected for acetic acid, benzoic acid, butylamine and glucose (Figures 5; Figure S5; Figures S11, S15 and S21; and Table S2).

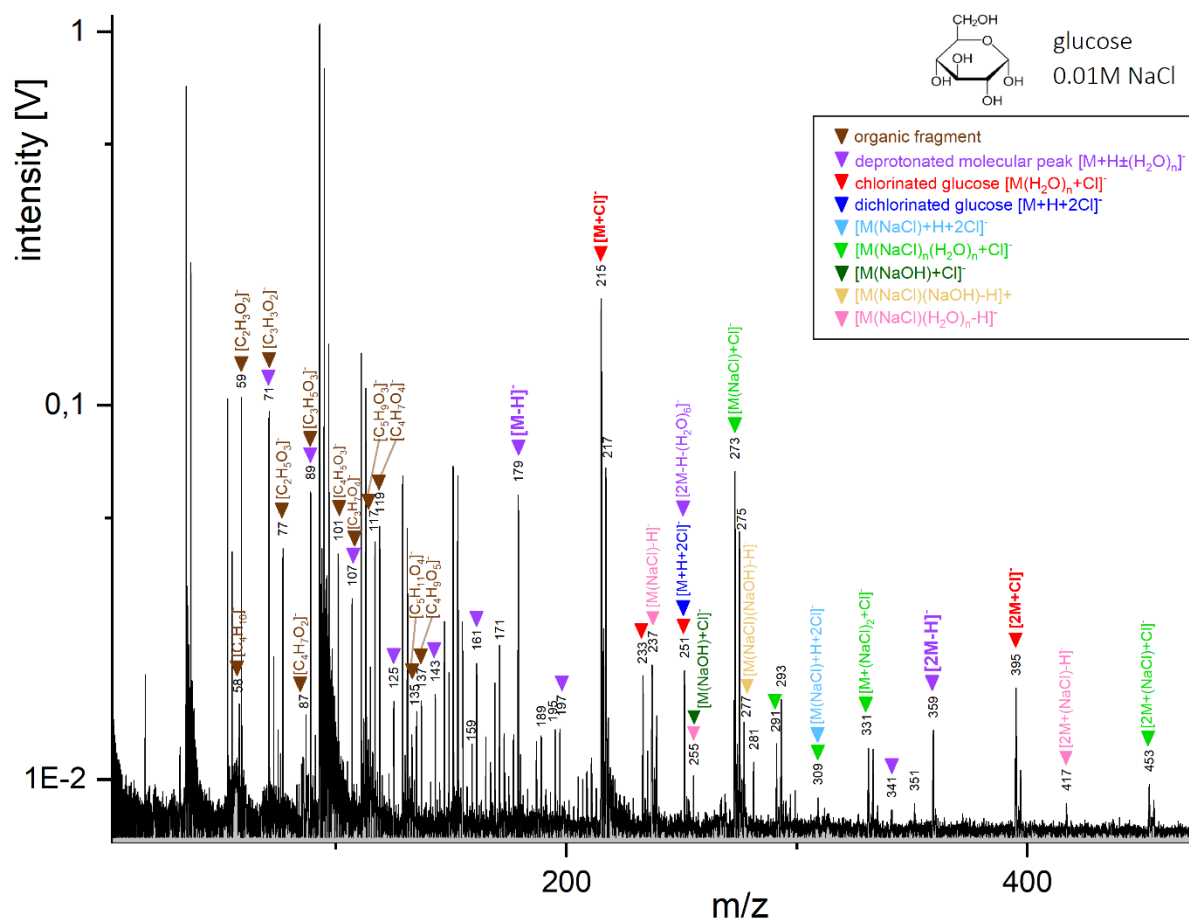


Figure 5. Baseline-corrected anion mass spectrum of glucose at a concentration of 5wt% in a H₂O and NaCl (0.01M) matrix, recorded at a delay time of 6.1 μs. Characteristic deprotonated molecular peak $[M-H]^-$ and chlorinated peak $[M+Cl]^-$ are labeled in purple and red, respectively, with their corresponding water clusters. Unlabeled peaks originate exclusively from the salty matrix. Peaks labeled in brown correspond to glucose fragments. Peaks labeled in all other colors were identified as salt adducts.

3.3.2 Intermediate Salt Concentration (0.1M NaCl)

At a concentration of 0.1M NaCl in the matrix solution, protonated molecular peaks ($[M+H]^+$) are much weaker than in a 0.01M NaCl matrix (e.g., Figures 4 and 6) but are still detectable for 5-amino-1-pentanol, butylamine and glucose (Table 2). Protonated molecular peaks are not detected anymore for acetic acid, benzoic acid, methanol, and pyridine. Sodiated molecular ions ($[M+Na]^+$) are detectable for all organics except acetic acid, at intensities lower than in 0.01M NaCl matrices (e.g., Figures S18 and S19). Clusters of sodiated organic molecules with NaCl ($[M(NaCl)+Na]^+$) were detected for all organics except acetic acid, usually at higher intensities than in 0.01M NaCl matrices (e.g., Figures 4 and 6). Clusters of sodiated organic molecules with NaOH ($[M(NaOH)+Na]^+$) were detected for 5-amino-1-pentanol, butylamine and pyridine, and tentatively detected for benzoic acid, at roughly similar intensities as compared to 0.01M NaCl matrices. Disodiated peaks ($[M-H+2Na]^+$) were detected in the cation mass spectra of 5-amino-1-pentanol, acetic acid, benzoic acid and glucose (Figure 6; Figures S9, S14 and S23), and trisodiated peak were detected for 5-amino-1-pentanol ($[M-2H+3Na]^+$) and acetic acid dimers ($[2M-2H+3Na]^+$). Whereas the disodiated peaks of benzoic acid had weaker intensities in 0.1M NaCl than in 0.01M NaCl matrices, the intensities of disodiated glucose peak were roughly similar in both matrices, and those of 5-amino-1-pentanol and acetic acid were stronger in 0.1M NaCl matrices. The trisodiated peak of 5-amino-1-pentanol was not present in 0.01M NaCl matrices, and that of the acetic acid dimer is much higher in 0.1M NaCl than in 0.01M NaCl matrices. Clusters of disodiated organic molecules with NaCl ($[M(NaCl)-H+2Na]^+$) were detected for acetic and benzoic acids. Compared to 0.01M matrices, a smaller number of fragments at lower intensities are usually detected (e.g. Figures 4 and 6). No $[M(NaCl)_n+H]^+$ peak was detected.

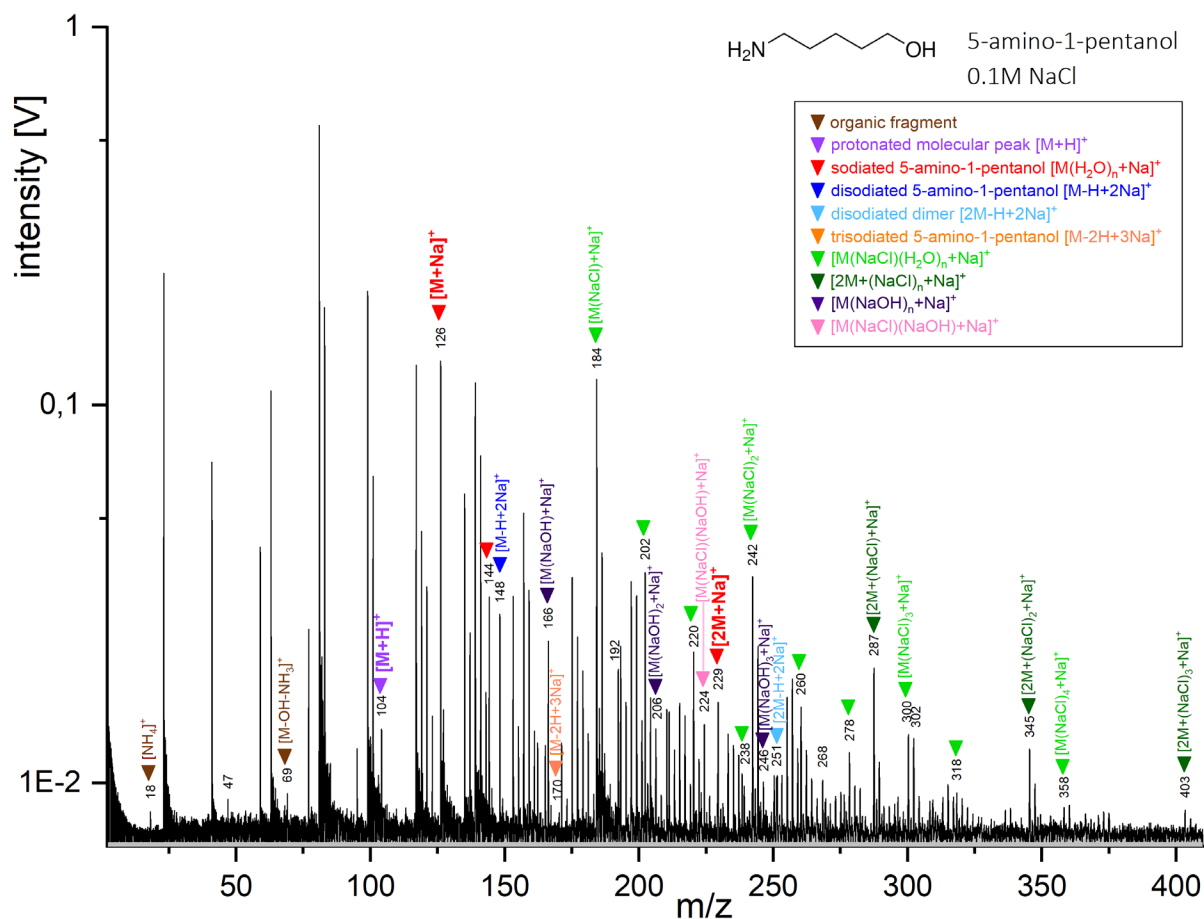


Figure 6. Baseline-corrected cation mass spectrum of 5-amino-1-pentanol at a concentration of 5wt% in a H₂O and 0.1M NaCl matrix, recorded at a delay time of 6.3 μ s. Unlabeled peaks originate exclusively from the salty matrix.

In anion mode, acetic acid, benzoic acid, and glucose were identified as deprotonated molecular ions ($[M-H]^-$), and 5-amino-1-pentanol, glucose, and methanol were identified as chlorinated ions ($[M+Cl]^-$) (Table 3), all at lower intensities as compared to 0.01M NaCl matrices (Figures 5 and 7; Figures S5, S6, S11, S12, S15, S16, S29, and S30). Salt adducts were detected for 5-amino-1-pentanol, acetic acid, benzoic acid, glucose, and methanol at intensities roughly similar to 0.01M NaCl matrices: $[M(NaCl)_n+Cl]^-$ for 5-amino-1-pentanol, glucose and methanol; $[M(NaCl)_n-H]^-$ for 5-amino-1-pentanol, acetic acid, benzoic acid and glucose; and $[M(NaOH)-H]^-$ and $[M(NaCl)_n(NaOH)-H]^-$ for glucose. As in the 0.01M NaCl matrix, sodiated

anion dimers $[2M-2H+Na]^-$ and disodiated anion trimers $[3M-3H+2Na]^-$ were detected in the spectra of acetic acid, at higher intensities as compared to 0.01M NaCl. Fragments of acetic acid, benzoic acid, butylamine and glucose were detected (Table S2).

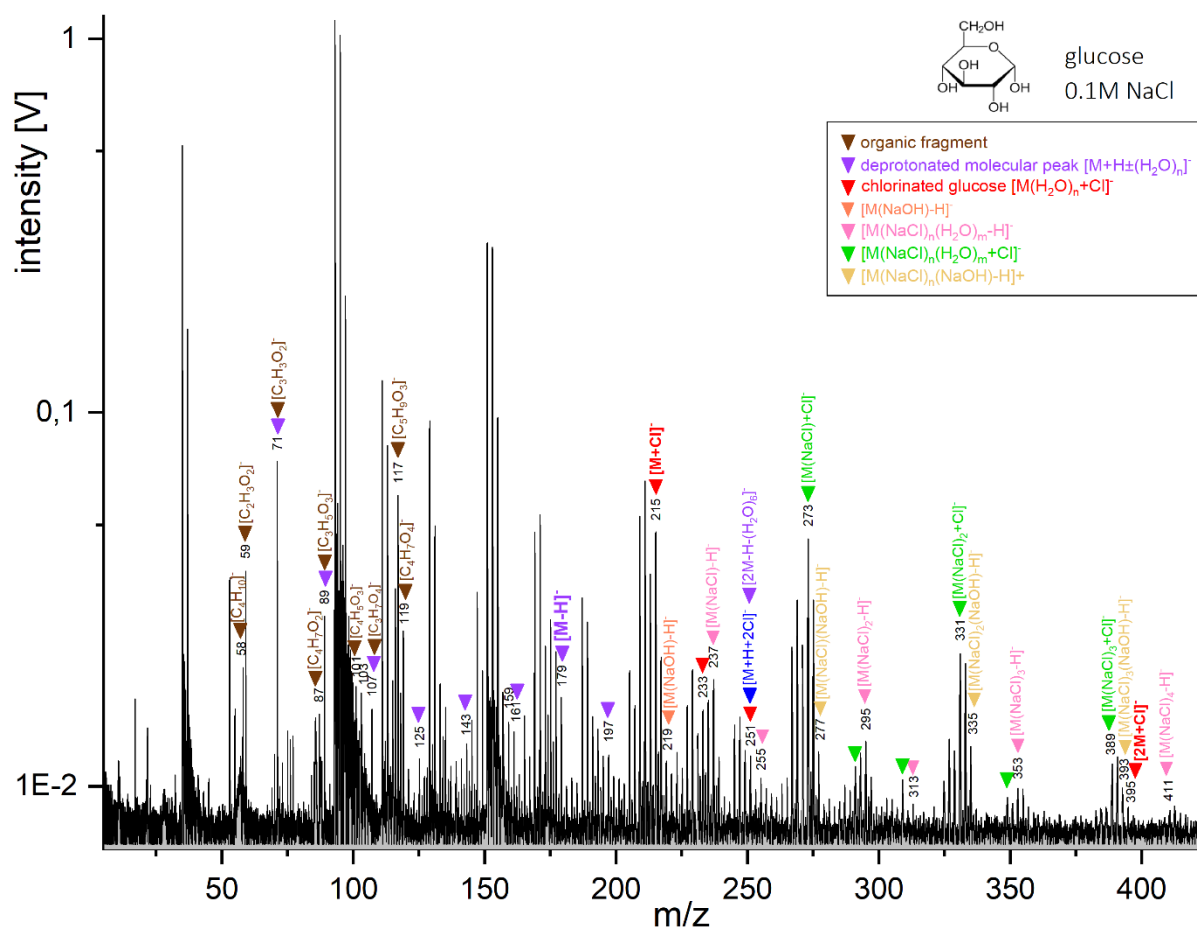


Figure 7. Baseline-corrected anion mass spectrum of glucose at a concentration of 5wt% in a H_2O and NaCl (0.1M) matrix, recorded at a delay time of $6.2\mu s$. Unlabeled peaks originate exclusively from the salty matrix.

3.3.3 High Salt Concentration (1M NaCl)

At a concentration of 1M NaCl, protonated molecular peaks ($[M+H]^+$) are detectable for 5-amino-1-pentanol (Figure 8) and glucose despite an interference with a salt cluster (Figure S25). Sodiated molecular ions ($[M+Na]^+$) are detected for 5-amino-1-pentanol, glucose, methanol and pyridine (Figure 8; Figures S25, S28 and S33). As compared to the 0.1M NaCl

matrix, protonated molecular peaks are not detected anymore for butylamine and sodiated peaks are not detected anymore for benzoic acid and butylamine. All detected protonated and sodiated peaks have lower intensities than in 0.1M NaCl matrices (e.g., Figures 6 and 8). Clusters of sodiated organic molecules with NaCl ($[M(\text{NaCl})+\text{Na}]^+$) were detected for all organics except acetic and benzoic acid, and at lower intensities than in 0.1M NaCl matrices. In the mass spectra of butylamine (Figure S20), $[M(\text{NaCl})_{1-2}+\text{Na}]^+$ clusters were detected although no $[M+\text{Na}]^+$ peaks were detected. $[M(\text{NaCl})+\text{Na}]^+$ clusters are the highest organic-related peaks in the mass spectra of 5-amino-1-pentanol, butylamine, pyridine, and methanol. Clusters of sodiated organic molecules with NaOH ($[M(\text{NaOH})+\text{Na}]^+$) were detected for 5-amino-1-pentanol, at lower intensities as compared to 0.1M NaCl matrices (Figures 6 and 8). Disodiated peaks ($[M-\text{H}+2\text{Na}]^+$) were detected in the cation mass spectra of 5-amino-1-pentanol, acetic acid, and glucose at similar (for acetic acid) or lower intensities as compared to 0.1M NaCl matrices. As compared to the 0.1M NaCl matrix, disodiated peaks were not detected for benzoic acid anymore. Trisodiated dimers ($[2M-2\text{H}+3\text{Na}]^+$) and clusters of disodiated organic molecules with NaCl ($[M(\text{NaCl})-\text{H}+2\text{Na}]^+$) were detected for acetic acid, both at lower intensities as compared to 0.1M NaCl matrices. Cationic fragments were only detected for glucose and 5-amino-1-pentanol (Figure S2 and, Table S1). Similarly to 0.1M NaCl matrices, $[M(\text{NaCl})+\text{H}]^+$ cations were not detected.

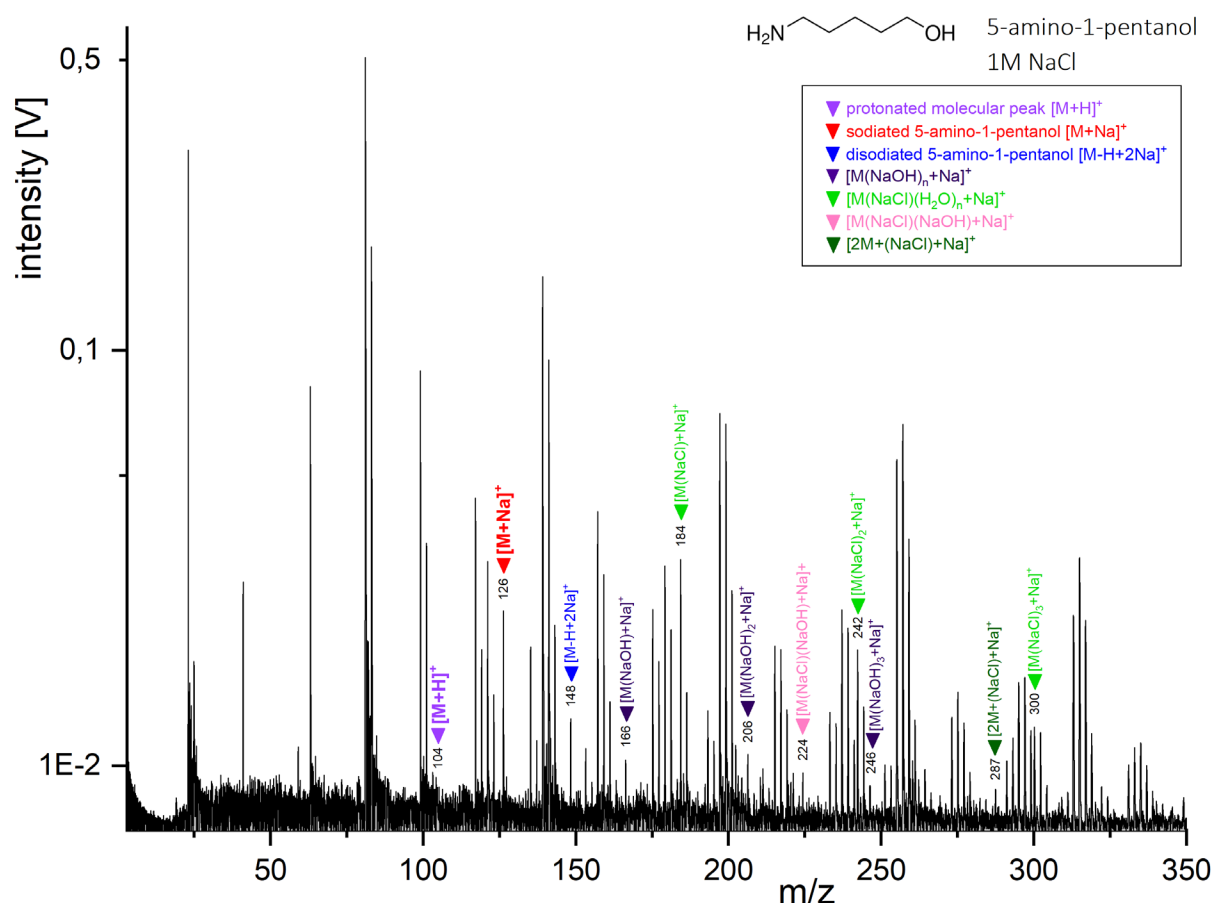


Figure 8. Baseline-corrected cation mass spectrum of 5-amino-1-pentanol at a concentration of 5wt% in a H₂O and 1M NaCl matrix, recorded at a delay time of 6.5 μ s. Characteristic protonated molecular peak [M+H]⁺ and sodiated peak [M+Na]⁺ are labeled in purple and red, respectively. Unlabeled peaks originate exclusively from the salty matrix. Peaks labeled in all other colors were identified as salt adducts.

In anion mode, only acetic acid and benzoic acid showed characteristic organic signatures, whereas the spectra of all other organics are similar to pure 1M NaCl spectra. For both acetic acid and benzoic acid, deprotonated molecular peaks were detected with a high sensitivity (Figure 9 and Figure S17), but at lower intensities than in 0.01M NaCl matrices. Salt adducts ([M(NaCl)_n-H]⁻) were detected for both acetic acid and benzoic acid, for both at lower

intensities as compared to 0.01M NaCl matrices. Clusters $[2M-H+(NaCl)_n]^-$, $[3M-H+(NaCl)_n]^-$, $[2M-2H+(NaCl)_n+Na]^-$ and $[3M-H+(NaCl)_n]^-$, were detected for acetic acid (Figure 9). One organic fragment was detected for acetic acid ($[CH_3]^-$) and benzoic acid (deprotonated benzene).

Detection limits were estimated in 1M NaCl matrices for the compounds with the highest sensitivities (i.e., 5-amino-1-pentanol in cation mode and acetic acid in anion mode). Deprotonated molecular ions of acetic acid were identified in a 1M NaCl matrix at a concentration as low as 0.1wt% (Figure S35). In cation mode, 5-amino-1-pentanol and glucose were the only organics that could be surely identified at 1M NaCl as a protonated molecular peak, at a concentration of 5wt% (Figure 8 and Figure S25). The protonated molecular peak of 5-amino-1-pentanol could not be observed at lower concentrations than 5wt%, but the sodiated peak was detected down to a concentration of 1wt% (Figure S36).

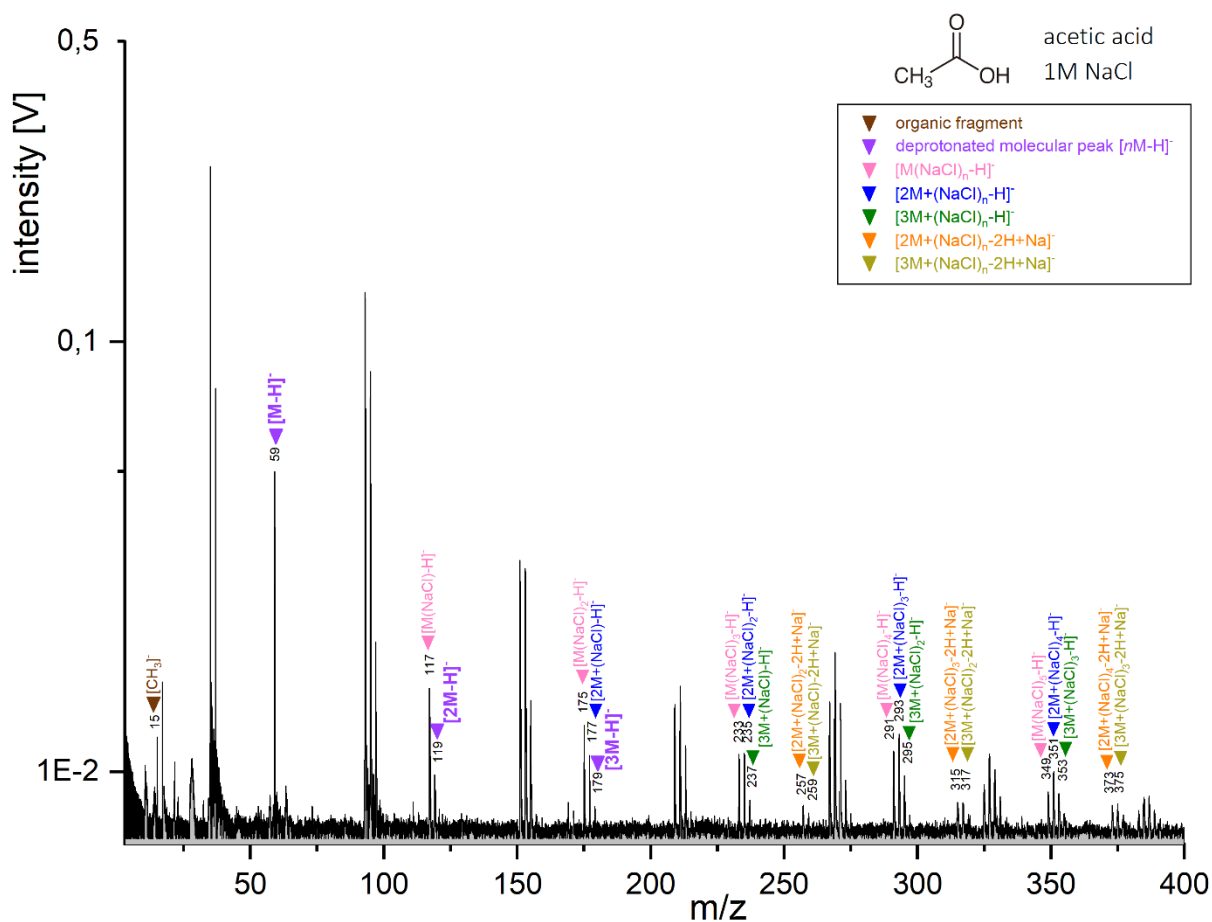


Figure 9. Baseline-corrected anion mass spectrum of acetic acid at a concentration of 5wt% in a H₂O and 1M NaCl matrix, recorded at a delay time of 6.5 μ s. Characteristic deprotonated molecular peaks [M-H]⁻ are labeled in purple. Unlabeled peaks originate exclusively from the salty matrix. Peaks labeled in brown correspond to organic fragments. Peaks labeled in all other colors were identified as salt adducts.

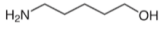
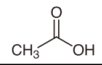
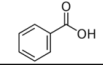
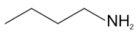
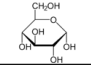
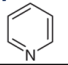
			5-amino-1-pentanol 	Acetic acid 	Benzoic acid 	Butylamine 	Glucose 	Methanol HO-CH ₃	Pyridine 
0.01M NaCl	[M+H] ⁺	<i>M+1 u</i>	✓	✓	✓	✓	✓	✓	✓
	[M+Na] ⁺	<i>M+23 u</i>	✓	✓	✓	✓	✓	✓	✓
	[M(NaCl)+H] ⁺	<i>M+59 u</i>		✓	✓				
	[M(NaCl)+Na] ⁺	<i>M+81 u</i>	✓	✓	✓	✓	✓	✓	✓
	[M(NaOH)+Na] ⁺	<i>M+63 u</i>	✓	✓	✓	✓			✓
	[M-H+2Na] ⁺	<i>M+45 u</i>	✓	✓	✓		✓		
	[M-2H+3Na] ⁺	<i>M+67 u</i>					✓		
	[2M-2H+3Na] ⁺	<i>2M+67 u</i>		✓					
	[M(NaCl)-H+2Na] ⁺	<i>M+103 u</i>		✓	✓				
0.1M NaCl	[M+H] ⁺	<i>M+1 u</i>	✓			✓	✓		
	[M+Na] ⁺	<i>M+23 u</i>	✓		✓	✓	✓	✓	✓
	[M(NaCl)+H] ⁺	<i>M+59 u</i>							
	[M(NaCl)+Na] ⁺	<i>M+81 u</i>	✓		✓	✓	✓	✓	✓
	[M(NaOH)+Na] ⁺	<i>M+63 u</i>	✓		✓	✓	✓		✓
	[M-H+2Na] ⁺	<i>M+45 u</i>	✓	✓	✓		✓		
	[M-2H+3Na] ⁺	<i>M+67 u</i>	✓						
	[2M-2H+3Na] ⁺	<i>2M+67 u</i>		✓					
	[M(NaCl)-H+2Na] ⁺	<i>M+103 u</i>		✓	✓				
1M NaCl	[M+H] ⁺	<i>M+1 u</i>	✓				✓		
	[M+Na] ⁺	<i>M+23 u</i>	✓				✓	✓	✓
	[M(NaCl)+H] ⁺	<i>M+59 u</i>							
	[M(NaCl)+Na] ⁺	<i>M+81 u</i>	✓			✓	✓	✓	✓
	[M(NaOH)+Na] ⁺	<i>M+63 u</i>	✓						
	[M-H+2Na] ⁺	<i>M+45 u</i>	✓	✓			✓		
	[M-2H+3Na] ⁺	<i>M+67 u</i>							
	[2M-2H+3Na] ⁺	<i>2M+67 u</i>		✓					
	[M(NaCl)-H+2Na] ⁺	<i>M+103 u</i>		✓					

Table 2. Detected Peaks, and Their Respective *m/z* Values, in Cation Mode for the Investigated Organics at 0.01M, 0.1M and 1M NaCl Concentrations. Blue symbols (✓) represent tentative identifications.


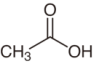
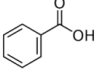
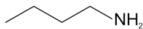
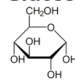
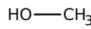
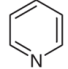
			5-amino-1-pentanol 	Acetic acid 	Benzoic acid 	Butylamine 	Glucose 	Methanol 	Pyridine 
0.01M NaCl	[M-H] ⁻	<i>M-1 u</i>	✓	✓	✓		✓		
	[M+Cl] ⁻	<i>M+35 u</i>	✓		✓		✓	✓	✓
	[M(NaCl)-H] ⁻	<i>M+57 u</i>	✓	✓	✓		✓		
	[M(NaOH)-H] ⁻	<i>M+39 u</i>					✓		
	[M(NaCl)+Cl] ⁻	<i>M+93 u</i>	✓		✓		✓	✓	
	[M(NaOH)+Cl] ⁻	<i>M+75 u</i>					✓		
	[M+H+2Cl] ⁻	<i>M+71 u</i>					✓		
	[2M-2H+Na] ⁻	<i>2M+21 u</i>		✓	✓				✓
	[3M-3H+2Na] ⁻	<i>3M+43 u</i>		✓					
0.1M NaCl	[M-H] ⁻	<i>M-1 u</i>		✓	✓		✓		
	[M+Cl] ⁻	<i>M+35 u</i>	✓				✓	✓	
	[M(NaCl)-H] ⁻	<i>M+57 u</i>	✓	✓	✓		✓		
	[M(NaOH)-H] ⁻	<i>M+39 u</i>					✓		
	[M(NaCl)+Cl] ⁻	<i>M+93 u</i>	✓				✓	✓	
	[M(NaOH)+Cl] ⁻	<i>M+75 u</i>							
	[M+H+2Cl] ⁻	<i>M+71 u</i>							
	[2M-2H+Na] ⁻	<i>2M+21 u</i>		✓					
	[3M-3H+2Na] ⁻	<i>3M+43 u</i>		✓					
1M NaCl	[M-H] ⁻	<i>M-1 u</i>		✓	✓				
	[M+Cl] ⁻	<i>M+35 u</i>							
	[M(NaCl)-H] ⁻	<i>M+57 u</i>		✓	✓				
	[M(NaOH)-H] ⁻	<i>M+39 u</i>							
	[M(NaCl)+Cl] ⁻	<i>M+93 u</i>							
	[M(NaOH)+Cl] ⁻	<i>M+75 u</i>							
	[M+H+2Cl] ⁻	<i>M+71 u</i>							
	[2M-2H+Na] ⁻	<i>2M+21 u</i>							
	[3M-3H+2Na] ⁻	<i>3M+43 u</i>							

Table 3. Detected Peaks, and Their Respective *m/z* Values, in Anion Mode for the Investigated Organics at 0.01M, 0.1M and 1M NaCl Concentrations. Blue symbols (✓) represent tentative identifications.

3.4. Detection of Organic Fragments

Organic fragments are crucial for spectral interpretation as they provide structural information and might help to resolve ambiguities from the molecular or cluster peaks alone. In water matrices, fragments were detected for all organic species in both ion modes, except for methanol in anion mode (Tables S1 and S2). In salt-rich matrices, organic fragments were detected in at least one ion mode for all the investigated organics except methanol and pyridine (Tables S1 and S2). The number of characteristic organic fragments, as well as their intensities, decreased with increasing NaCl concentration (Tables S1 and S2). The fragments observed at high NaCl concentrations were usually also observed at low NaCl concentrations.

Both 5-amino-1-pentanol and butylamine formed cationic fragments by losing their functional groups, typically forming $[\text{NH}_4]^+$, $[\text{CH}_2\text{NH}_2]^+$ and/or $[\text{CH}_2\text{O}]^+$, $[\text{M-OH-NH}_3]^+$ and $[\text{M-OH}]^+$ fragments for 5-amino-1-pentanol, and $[\text{NH}_4]^+$ and $[\text{M-NH}_2]^+$ fragments for butylamine.

Both acetic acid and benzoic acid formed $[\text{M-OH}]^+$ peaks in 0.01M NaCl matrices, but different cationic fragments are detected at higher NaCl concentrations: at 0.1M NaCl, $[\text{CO}]^+$ is detected for acetic acid and $[\text{C}_3\text{H}_3]^+$ for benzoic acid. No fragments are detected at higher NaCl concentration in cation mode. In the anion mass spectra of acetic acid, $[\text{CH}_3]^-$ fragments were detected at all NaCl concentrations at approximately similar intensities (Figure 9 and Figures S11, S12). Deprotonated benzene ($[\text{M-COOH}]^-$) was detected in the anion mass spectra of benzoic acid at all NaCl concentrations, at intensities decreasing with increasing NaCl concentrations (Figures S15-S17).

A high number of glucose fragments were detected in cation mode at all NaCl concentrations (Table S1), and in anion mode at 0.01M and 0.1M NaCl (Table S2). Fragments resulted from the successive loss of water from the alcohol functional groups of the deprotonated glucose molecule and other fragmentation pathways (e.g., Figure 10). As other compounds containing hydroxyl (-

OH) groups, glucose typically form $[M-OH]^+$ fragments. Glucose is the only organic for which a high number of fragments was detected in 1M NaCl matrices.

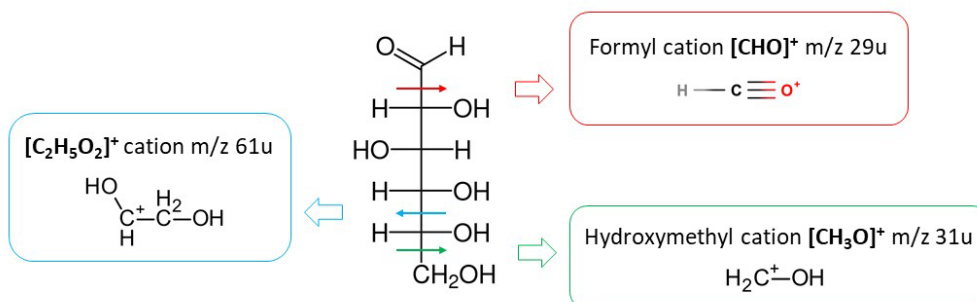


Figure 10. Examples of fragmentation pathways of some detected cation fragments of glucose. The arrows represent bond cleavage.

3.5. General Trends

Our results show that organics embedded in high-salinity ice grains can still be detected because of the formation of molecular ions and sodiated and chlorinated adducts. However, the spectral appearance of the organics fundamentally changes from relatively low (0.01M) to high (1M) NaCl matrices. The formation, and relative intensities, of different ions and salt adducts at varying salt concentrations strongly influence the resulting spectra. Organic molecular peaks but also sodiated and chlorinated organic adducts are effectively suppressed with increasing NaCl concentrations, and the relative intensities of peaks change with varying salt concentrations.

Suppression Effects

Effective suppression effects by the salt^{67,71} provoked a general decrease of the absolute number and intensities of organic-related peaks, including molecular peaks, fragment peaks and sodiated and chlorinated peaks, with increasing NaCl concentration in both ion modes (Figures 11 and 12, Tables 2 and 3, and Tables S1 and S2). We investigated the trends of the amplitudes of protonated and sodiated peaks (Figure 11) and of (de)protonated molecular peaks (Figure 12) in matrices of increasing NaCl concentration, by normalizing these peaks' integrals against the total integrated ions. This analysis showed that the degree of suppression of molecular peaks as well as some

sodiated and chlorinated peaks by the salt is highly dependent on the organic species and ranges from less than a factor of 2 up to several orders of magnitude. Figures 11 and 12 should nonetheless be treated cautiously, because they don't represent true comparisons of ionization efficiencies between the different organic species: multiple variables have an influence on the peak amplitudes (e.g., the organic/NaCl ratio is decreasing in the solution as [NaCl] increases; the different organic samples have different molecular densities). Rather than an absolute quantitative comparison, Figures 11 and 12 provide valuable trends representative of suppression effects for a variety of organic species. The amount of water clusters, in the spectra of both pure NaCl matrix and organic-rich salty solutions, decreased with increasing NaCl concentration. Counterintuitively, the number and intensities of both sodiated and chlorinated peaks were also found to likewise decrease with increasing NaCl concentration (e.g., Figures 4-8).

By contrast, intensities increased with salinity for clusters of sodiated organic molecules with NaCl ($[M(\text{NaCl})+\text{Na}]^+$).

Ion Mode

Most of the organics investigated typically formed a larger number of peaks in cation mode than in anion mode (Tables 2 and 3). Generally, we observe a trend of lower response of the organics in anion mode as compared to cation mode. Whereas all organics formed protonated and sodiated molecular peaks (at least in 0.01M NaCl matrices), only some of the organics formed deprotonated or chlorinated peaks. The intensities of organic peaks are usually higher in cation mode than anion mode, except for the two carboxylic acids, to which the sensitivity was much higher in anion mode than cation mode. These two species are the only organics that were detected at the highest NaCl concentration (1M) in anion mode, thanks to highly significant deprotonated molecular peaks (Figure 9 and Figure S17). In anion mode, the response of the different organics varied greatly from one organic species to another. In particular, butylamine and pyridine are not or barely detectable even at low NaCl concentrations.

Sodiation and Chlorination Processes

Sodiation appears to play a major role in the spectral appearance of the organics in salt-rich matrices. In cation mode spectra, the most prevalent characteristic peaks are sodiated peaks ($[M+Na]^+$) for all organics, except for acetic acid and benzoic acid for which disodiated peaks $[M-H+2Na]^+$ dominate (Figures S7-S10, S13 and S14). A higher absolute number of sodiated species have been detected for acetic acid and benzoic acid (e.g., $[M(NaCl)-H+2Na]^+$, $[2M-2H+Na]^+$; Tables 2 and 3), and for acetic acid only ($[3M-3H+2Na]^+$, $[4M-3H+2Na]^+$, $[xM-2H+Na]^+$, $[xM-3H+2Na]^+$ and $[4M-4H+3Na]^+$; Table 3, Figures S11 and S12), as compared to other organics. Disodiated cations $[M-H+2Na]^+$ have been detected for all species containing hydroxyl (-OH) functional group(s) except methanol (i.e., 5-amino-1-pentanol, acetic acid, benzoic acid and glucose), but at much higher intensities for acetic acid and benzoic acid as compared to the other organics. Trisodiated cations have been detected for glucose ($[M-2H+3Na]^+$) and acetic acid dimers and trimers ($[2M-2H+3Na]^+$, $[3M-2H+3Na]^+$). Chlorination processes (i.e., addition of a chloride anion) were also observed: chlorinated peaks ($[M+Cl]^+$) were detected in 0.01M NaCl matrices for most organics, and dichlorinated peaks ($[M+H+2Cl]^+$) were tentatively detected for glucose in 0.01M NaCl matrix.

Salt Clusters with NaCl and NaOH

A variety of salt clusters were observed in both ion modes. Clustering of NaCl onto cations or anions was observed more frequently, and create higher intensity peaks, than clustering of NaOH in both ion modes. This is consistent with the spectra of the pure NaCl matrix, where clusters of $[Na(NaCl)_n]^+$ and $[Cl(NaCl)]^-$ are much more significant than $[Na(NaOH)_n]^+$ and $[Cl(NaOH)_n]^-$ (Figures 2 and 3 and Figures S1-S4). Clustering of NaCl onto sodiated molecules ($[M(NaCl)_n+Na]^+$) appeared to be more frequent than onto protonated molecules ($[M(NaCl)_n+H]^+$). The relative intensity of $[M(NaCl)_n+Na]^+$ in many cases increased with NaCl concentrations (e.g., Figures 4, 6 and 8), although the intensities of $[M+Na]^+$ peaks decreased. Conversely, clusters of protonated organics with NaCl ($[M(NaCl)+H]^+$) were detected only in

0.01M matrices but not at higher NaCl concentrations. At 1M NaCl concentrations, $[M(\text{NaCl})+\text{Na}]^+$ peaks were detected for butylamine although sodiated peaks $[M+\text{Na}]^+$ were not detected. In anion mode, both $[M(\text{NaCl})_n-\text{H}]^-$ and $[M(\text{NaCl})_n+\text{Cl}]^-$ clusters were detected for many organics, but clustering of anions with NaOH was only observed for glucose.

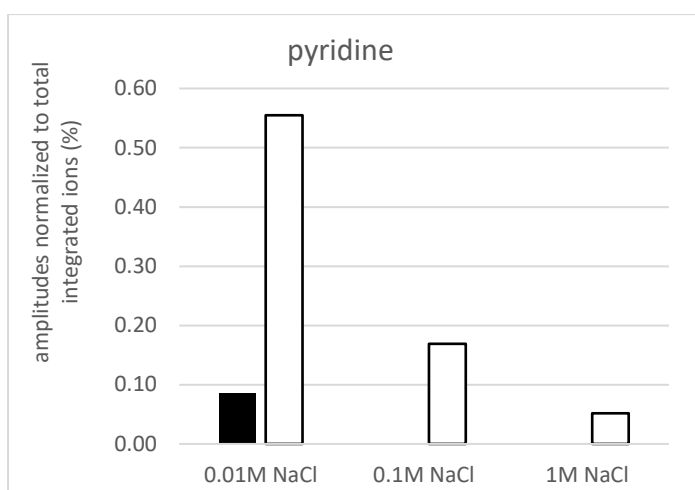
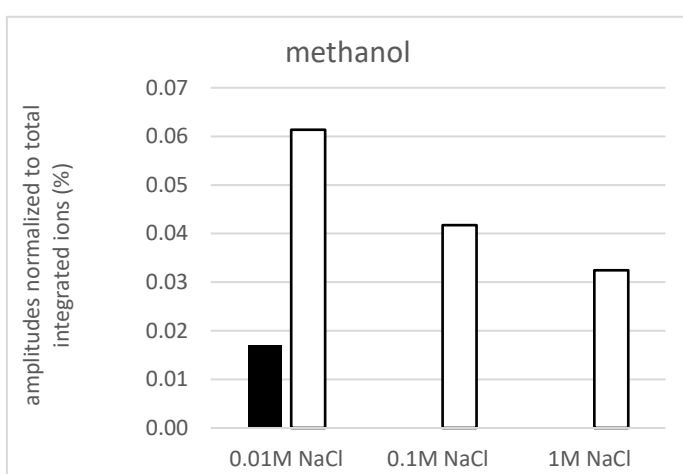
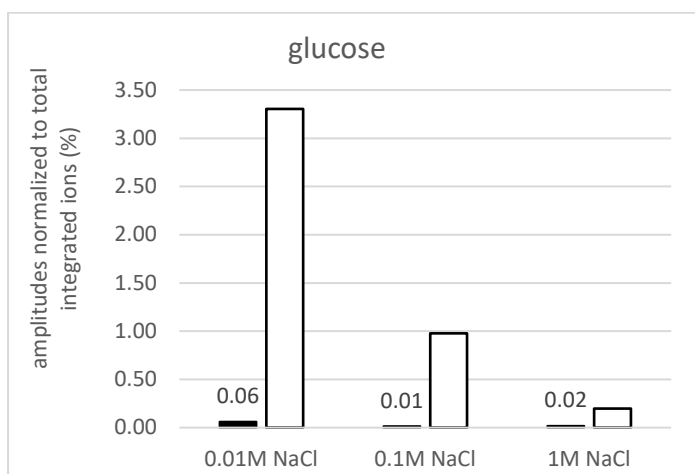
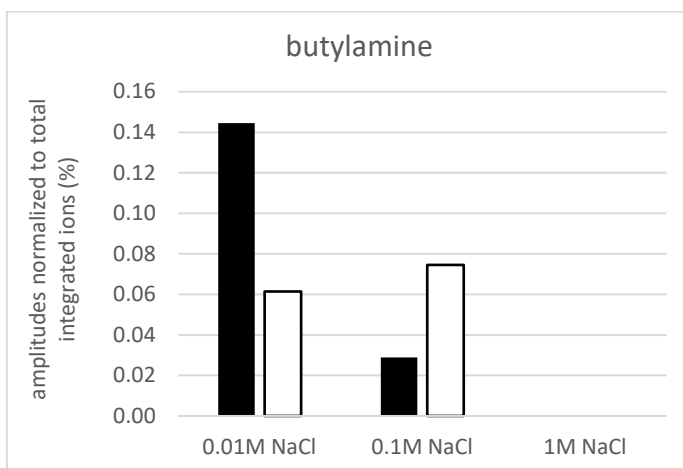
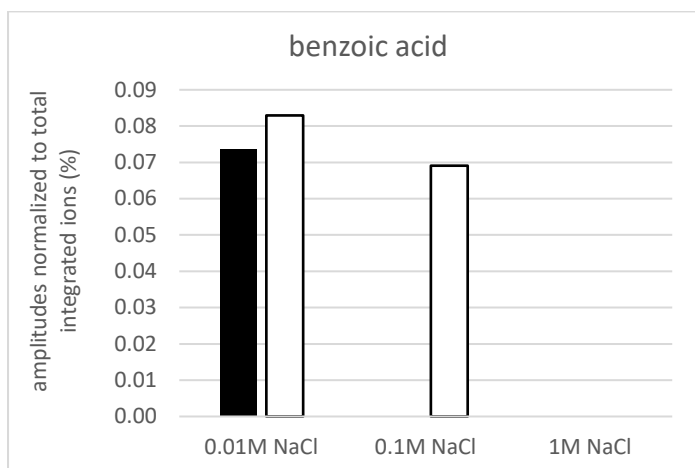
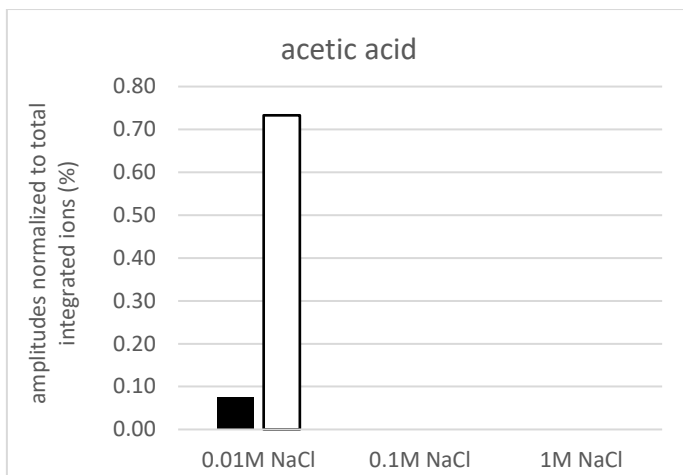
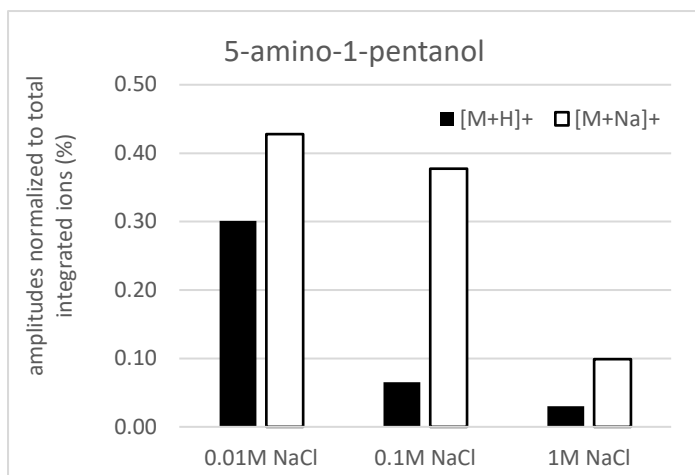


Figure 11. Relative amplitudes of protonated molecular peaks $[M+H]^+$ and sodiated peaks $[M+Na]^+$ in 0.01, 0.1 and 1M NaCl matrices for the seven measured organic species. Peak amplitudes were normalized to the total integrated ions.

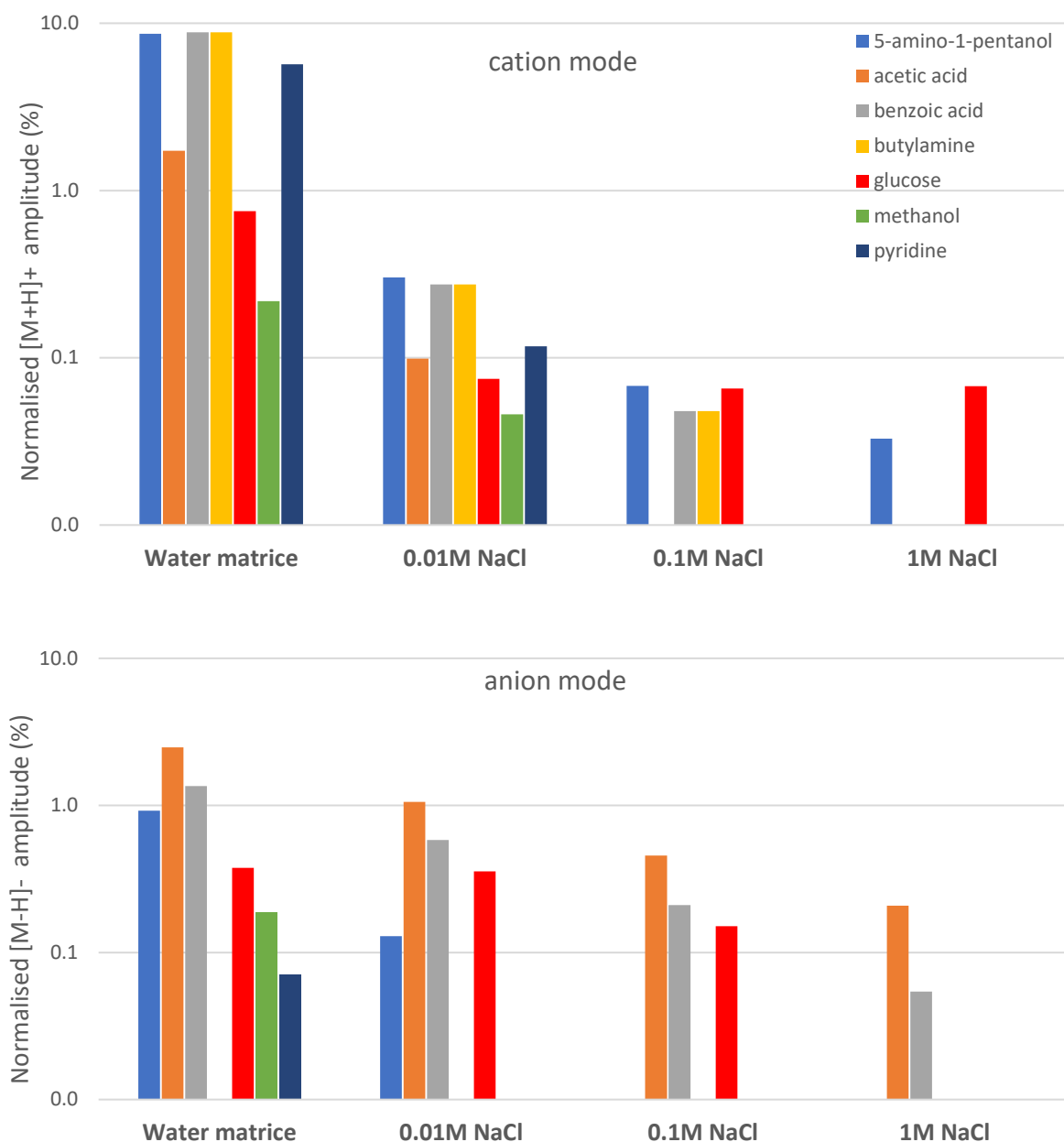


Figure 12. Relative amplitudes of protonated molecular peaks $[M+H]^+$ (top) and deprotonated molecular peaks $[M-H]^-$ (bottom) in water matrices and 0.01, 0.1 and 1M NaCl matrices for the seven organic species measured in cation and anion mode. Amplitudes were normalized against the integral of the whole spectra and plotted on a logarithmic scale.

4 Discussion

In this work, we performed analogue experiments for the detection of organic molecules in salt-rich ice grains from icy moons with impact ionization mass spectrometry. A range of organic compounds were measured with the LILBID setup in water and NaCl-rich matrices at different salt concentrations (0.01, 0.1 and 1M NaCl). Our results show that our laboratory setup is more sensitive to the majority of the measured organics and their fragments in the cation mode than in the anion mode. The sensitivity in negative ion mode has also been reported to be generally lower than that in positive ion mode in both Matrix Assisted Laser Desorption Ionization mass spectrometry (MALDI)-MS^{78, 79} and electrospray ionization (ESI)-MS⁸⁰. The lower sensitivity in anion mode must be due to differences in mechanisms leading to the formation of charged analyte molecules during the ionization process, which are not yet very well understood. Anions can be generated by (i) deprotonation from the analyte, (ii) fragmentation during the ionization process, (iii) adduct formation with anions, or (iv) simultaneous deprotonation and adduct formation with cations (e.g., $[2M-2H+Na]^-$ ions). Analytes with free electron pairs can be easily ionized by the attachment of protons and cations (e.g., $[M+Na]^+$).

Different organic species have different ionization efficiency that depends on the organic's intrinsic properties⁸¹. The organic response depends on its molecular structure and on its physicochemical properties. Using the LILBID setup, Klenner et al.⁶⁶ found a better sensitivity to amino acids in the cation mode than in the anion mode. Basic amino acids with high proton affinities have efficient proton transfer and therefore promote an efficient formation of cations. Generally, basic analytes often have lower sensitivities in negative ion mode than their corresponding protonated species in cation mode⁸². On the contrary, strong acids have higher ionization efficiency and give higher signals in the negative mode than in the positive mode, as shown by Kruve et al.⁸³ using ESI-MS. We found that the molecular structure of the organic

species and the presence of functional groups influence the ionization efficiency, the fragmentation pathways, and the formation of adducts:

- hydroxyl (OH) functional groups increase the ionization efficiency to form molecular anions. They also promote the formation of sodiated species, with protons from the hydroxyl functional groups being easily replaced by Na^+ , and allow the formation of characteristic $[\text{M-OH}]^+$ fragments, which often have a very prominent intensity, even higher than molecular peaks in some cases (e.g., for glucose; Figures S24 and S25).
- carboxylic acid functional groups (COOH) greatly increase the ionization efficiency to form deprotonated molecular anions. Such functional groups can be easily cleaved from the carboxylic acid-bearing molecule, leading to the formation of $[\text{M-COOH}]^-$ anions. They also promote sodiation processes, leading to the formation of both sodiated cations and anions. In cation mode, $[\text{M-H}+2\text{Na}]^+$ peaks are highly prominent, and much higher than $[\text{M}+\text{Na}]^+$. In water matrices, $[\text{M-OH}]^+$ fragments are the most prominent peaks in cation mass spectra (Figures S39 and S41).
- amine functional groups (NH_2) were found to decrease the ionization efficiency of molecular species in anion mode. Similarly to hydroxyl groups, they also promote the formation of sodiated species, with protons from the NH_2 being easily replaced by Na^+ .
- the presence of aromatic rings increases the stability of the molecular structure, inhibiting its fragmentation and the formation of respective fragment ions.
- species with a low pH show a very high signal in the anion mode and show significantly high deprotonated molecular peaks, even at high salt concentration.
- high pH species might be better detected in cation mode than anion mode, as seen in the anion mass spectra of 5-amino-1-pentanol, butylamine and pyridine that show very low signal.

Comparing butylamine and 5-amino-1-pentanol, i.e., two species with the same pH value of 12, we suggest that 5-amino-1-pentanol might have a better detectability than butylamine owing to its hydroxyl functional group. With the aim to detect specific types of organics, their pH values are a first important consideration when preferring negative or positive mode analysis. However, we could not establish a straightforward trend of detectability of all organics in relation to the pH, suggesting that the pH is only one important parameter among others, such as the presence of functional groups or the ion mode. This is in accordance with a study by Liigand et al.⁸⁴ that showed that decreasing pH can significantly increase the ionization efficiency of a compound, although other physicochemical properties, such as the pka, the number of potential charge center and the hydrogen bonding acceptor capacity were also found to play an important role in the analyte behavior.

In our experiments, the ionization efficiency of an organic species is related to the molecular density in the ionization region of the sample, therefore it depends on the organic's molecular concentration. The organics investigated have molar masses ranging from 32 to 180 g/mol (Table 1). In a constant volume V , the molecular density D of an organic species of mass m decreases when the molecular mass M increases ($D = \frac{m}{M \times V}$), e.g., glucose (M=180 g/mol) has a lower molecular density than methanol (M=32 g/mol). Molecular densities of the investigated organics therefore vary by a factor of ~6 between the lowest and the highest molecular masses organics. However, we believe that this effect has a second-order significance on the sensitivity as compared to the organics' intrinsic properties such as the pH or some specific functional groups.

Our results emphasize the need of both ion modes for future spaceborne impact ionization mass spectrometers because different organic families have different sensitivities in cation compared to anion mode. For example, the sensitivity to carboxylic acids is very high in anion mode even

at the highest salt concentration (Figure 9 and Figure S17); whereas butylamine, and pyridine at $C_{\text{NaCl}} > 0.01\text{M}$, could be detected in cation mode but not in anion mode (Tables 2 and 3). Measurements in both ion mode are therefore necessary to cover the complete range of the characteristic spectral signatures investigated here. Severe ion suppression as described here could result in false-negative results for samples containing organics. Both SUDA and ENIA will be capable of detecting both cations and anions^{38, 68}.

Whereas (de)protonated molecular peaks are the strongest peaks in pure water solutions, salt adducts instead form the strongest signals when salts are added to the matrix. Our results indicate that uncomplexed organics may be less stable than respective sodium complexes formed in a salt-rich solution, in agreement with previous mass spectrometry studies showing that sodium adducts can be difficult to fragment^{85, 86}. Sodiation of organic species is a well-known process in mass spectrometry^{67, 87}. The presence of hydroxyl (OH) and amine (NH₂) functional groups in the organic species' molecular structure promotes sodiation processes, as the protons from these functional groups can easily be replaced by a sodium cation (Na⁺), forming disodiated cations ([M-H+2Na]⁺) or in the case of several functional groups, polysodiated cations [M-mH+nNa]⁺ with m=n-1, e.g., trisodiated cations [M-2H+3Na]⁺. Sodiated organics [M-nH+mNa]^{(m-n)+} have been observed in ESI-MS and MALDI-MS, on a number of functional groups including amines, carboxylic groups and amides⁸⁸⁻⁹⁰. Interestingly, we detected a disodiated monomer ([M-H+2Na]⁺) and a trisodiated dimer ([2M-2H+3Na]⁺) in the mass spectra of acetic acid, and trisodiated cations were detected also for glucose ([M-2H+3Na]⁺), confirming that multiple functional groups are needed for multiple replacement of H atoms with Na⁺. Generally, the degree of sodiation of organic molecules depends on the number of hydroxyl and amine functional groups available in the organic molecule. The spectra of the two carboxylic acids show especially prominent disodiated cation peaks ([M - H + 2Na]⁺) as compared to other organics and sodiated anions were not detected

for any other organics, suggesting that carboxylic functional groups are even more efficient in incorporating Na^+ cations than hydroxyl groups that do not belong to carboxyl groups.

We observed chlorinated species for the first time with the LILBID, where a chloride anion is added in the molecular structure. Chlorinated species were detected for different families of organic species, but they were particularly prominent for glucose and methanol. Moreover, dichlorinated peaks ($[\text{M}+\text{H}+2\text{Cl}]^-$) were tentatively identified for glucose (Figure 5), suggesting that hydroxyl functional groups may offer favorable sites for chlorination to happen. Chlorination of organic species has also been previously observed in ESI and Orbitrap mass spectrometry^{91, 92}. The chlorinated peaks we observed were not as strong as sodiated peaks. Chloride attachment and more generally ionization by addition of anions, is a substantially softer form of ionization than with cations⁹³, because bonds between anions and molecules are usually weaker than corresponding bonds to cations (i.e., molecular proton affinities are usually higher than anion affinities).

Organic-related peaks tend to be fewer and have smaller intensities with increasing NaCl concentrations, due to suppression effects (so-called “salt-in” effects)^{67, 71, 94}. The degree of suppression varied from one sample to another, consistent with the expectation that suppression effects by salts are compound-dependent and concentration-dependent⁹⁵. Severe ion suppression has led to the non-detection of some organics, especially in anion mode and at high NaCl concentrations. We evaluated the strength of ion suppression by comparing the signal of molecular peaks of the analytes measured in pure water to their signal in increasing NaCl concentration matrices (Figure 12). The signal decreased by several orders of magnitude between pure water matrices and 1M NaCl matrices in both ion modes. The signals of sodiated peaks were also found to decrease drastically with increasing NaCl matrix concentration (Figure 11). However, the ion suppression cannot strictly be quantitatively estimated as in

Figures 11 and 12, the decrease in amplitude is likely to be due not solely to suppression effects, but also to other intertwined factors (e.g., the molar concentration). Suppression effects are caused by the general inhibition of ion formation at high salinities⁷⁶ and by the formation of sodiated and chlorinated adducts, which contributes to the reduction of signal of the (de)protonated organic species and results in loss of resolution and sensitivity⁹⁶. The formation of salt adducts spreads the un-sodiated molecular organic ions' signal over multiple different masses, causing a suppression of the signal of the analyte together with reduced detection abilities. Salt clusters can also increase the baseline noise, further lowering the signal-to-noise ratio.

Our results indicate that the detection and identification of organics in the mass spectra of salty grains are likely to be more difficult than for the salt-poor grains. At the highest NaCl concentration investigated (1M), most organics can only be detected as sodiated complex in cation mode, and cannot be detected at all in anion mode. However, several organic species i.e. low pH organics can still be detected even at 1M NaCl. High concentrations of salts as expected on Europa (0.1-1.2M NaCl)⁷ or Enceladus (0.05–0.2M NaCl)¹² could therefore degrade the spectral quality of organic-rich ice grains measured by impact ionization mass spectrometers. However, salts are not expected to always be present in every ice grain that carries organics (e.g., “Type 2” salt-poor, organic-rich ice grains from Enceladus ocean)⁹⁷, so the salt-in effects we describe are not applicable to all mass spectra recorded by spaceborne mass spectrometers. Ion suppression effects influencing the measurements of SUDA-type instruments might be stronger in cases where organic analytes are present only in trace amounts, because the potential for ion suppression in complex matrices is higher at low organic concentrations⁹⁸. However, high organic concentrations, perhaps on the order of several %, are expected on certain regions on Europa⁹⁹ i.e., chaos terrains¹⁰⁰. Moreover, the SUDA instrument will have a substantially higher dynamic range, together with a higher sensitivity,

than the mass spectrometer of our LILBID setup^{38, 68}, meaning that detection limits can be expected to be at least 1 order of magnitude lower than the detection limits we estimated and this might help counteracting the degradation of the spectral quality by salt-in effects. This increase in sensitivity would be even higher for future instruments investigating ice grains in the Enceladus plume, such as ENIA^{68, 101, 102}.

During impact ionization processes, kinetic energy is imparted to the molecules, and can be effectively released by the molecule breaking into fragments. Fragments have been detected for most of the investigated organics and in some cases, even at high salt concentrations (Tables S1 and S2). This is a new result as compared to previous studies by Klenner et al.^{66, 67}, where characteristic amino acid fragments were observed in salt-poor solutions but not in salt-rich solutions with a similar salinity (0.1M NaCl + 0.015M Na₂CO₃ + 0.015M NaHCO₃) as in our cases with fragment detection – but Klenner et al.⁶⁷ investigated amino acids at concentrations < 0.1%, which might be the reason why they did not observe fragments. However, we detected fewer characteristic organic ionic fragments with increasing salt concentrations. Judging from our results, the effectivity of the suppression of fragment ions depends on the analyte species, on its molecular structure and functional groups, and on the matrix salt concentration: fragmentation is inhibited for smaller organic molecules, with few functional groups, and is less likely at high NaCl concentrations. Among the investigated organics, glucose was found to form many fragments even at high NaCl concentrations. This may be due to its large molecular mass allowing the cleavage of many different bonds, and to its numerous hydroxyl functional groups that can easily be cleaved in an ionic form from the deprotonated glucose molecule. Both 5-amino-1-pentanol and butylamine were observed to form some of the same fragments reported by Klenner et al.⁶⁶ for amino acids, such as [NH₄]⁺ at m/z 18 and [CH₂NH₂]⁺ at m/z 30. Benzoic acid formed deprotonated benzene at m/z 77, consistent with the results of Klenner et al.⁶⁶ who showed that several amino acids typically cleaved their

carboxylic group to form $[M-COOH]^-$ anions. $[M-OH]^+$ fragments are typically detected for species containing hydroxyl functional groups. Fragments of pyridine and methanol were not detected in any salt-rich matrices. In the case of pyridine, the stability of its aromatic ring structure prevents fragmentation processes of the pyridine molecule. In the case of methanol, the small size of this compound (CH_3OH , 46u) does not allow the formation of many fragments, as compared to larger molecules.

The suppression of organic fragment ions at high salinities might be because the ionization of fragments is suppressed - alternatively, charged fragments may be neutralized by the salts, or the fragmentation process of the organics may be suppressed. NaCl has been shown to have a stabilizing effect against fragmentation in ESI mass spectrometry ^{e.g., 103}. Besides, we detected more fragments in cation than anion mode (Tables S1 and S2). This is consistent with the generally higher sensitivity to organic cations than organic anions that we observed, which then also applies to fragments. We did not detect sodiated fragments, although we expected them to form as results of the loss of water and functional groups from sodiated organics. Sodiated fragments have been observed in ESI mass spectrometry experiments ¹⁰⁴. Chlorinated fragments have also not been detected. This may suggest that sodiated and chlorinated species are more resistant to fragmentation than protonated and deprotonated molecular species, thanks to a stabilization by the salt that, in turn, hinder fragmentation; or that, alternatively, they form neutral fragments that we could not detect.

The sensitivity to the signal of the organics and their detection limits vary with the simulated impact speeds (i.e., combination of delay time and laser energy) ⁶⁴, the organic species, the salt concentration, and the ion mode. Detection limits were found to increase with increasing NaCl concentrations and were estimated at the highest salt concentration (1M NaCl). In anion mode, the most sensitive compounds were the two carboxylic acids, with acetic acid (the lowest pH

species) forming a deprotonated molecular peak at a concentration as low as 0.1 wt% (Figure S35). In cation mode, a save detection was established at 1wt% for 5-amino-1-pentanol. Our estimated detection limits in 1M NaCl (1000 ppmw in best case scenario) are, as expected, higher than those found by Klenner et al.⁶⁷ for amino acids in 0.1M NaCl matrices (between 0.5ppmw and 1000ppmw). Whereas Dannenmann et al.⁶⁹ detected bacterial biosignatures in low concentrations in salt-rich solutions up to 10⁻²M NaCl, our results show that the detection of other organics and potentially other types of biosignatures is possible at higher salt concentrations.

Our results provide insights into the behavior of organics in salt-rich solutions and therefore might help in the potential detection of organic biosignatures from ocean worlds. In particular, we investigated a sugar, glucose, and a N-heterocycle, pyridine, which are from important families for astrobiology investigations as they are typically found in biogenic material. Results from Dannenmann et al.⁶⁹ showed that deprotonated biomolecules can be unambiguously detected in 0.01M NaCl solutions. Salt-complexed adducts appear as reliable biosignatures that are more likely to be detected than (de)protonated biomolecules in an ocean world scenario. The wide range of compounds that we investigated allowed for a broader characterization applicable to other classes of (potentially yet unknown) biosignature molecules. The salt adducts we recurrently identified (Tables 1 and 2) for organics in NaCl-rich solutions, together with typical fragments (Tables S1 and S2), can allow the identification of unknown species in complex salt matrices. Larger organic molecules than the species we investigated could potentially be detected as organics contained in ice grains as they should be able to survive impact processes at velocities comparable to Europa Clipper flybys speeds^{15, 67, 105}, i.e., 4-5 km/s. Thanks to the protective effect of the ice matrix for large organics, even slightly higher impact speeds might be suitable.

Different impact speeds of ice grains onto impact ionization mass spectrometer detectors can be reproduced by selecting appropriate laser power density and ion extraction parameters (i.e., delay time of the gating system) on the LILBID setup ⁶⁴. The experimental parameters used here (laser intensities 97-100%; delay time 5.5-6.8 μ s) are compared to those required to simulate different impact speeds of water ice grains and are representative of a speed regime of around 4-8 km/s. This range of equivalent impact speeds lies within the range matching the maximum of detection sensitivity of amino acids, fatty acids and peptides ^{66, 67}.

5 Conclusions and Outlook

Both Europa and Enceladus have perhaps the highest potential of any extraterrestrial bodies in our Solar System to host extant biological life. Their oceans and surface ice are expected to contain sodium chloride (NaCl) salt among their major non-water constituents ^{e.g., 12, 55, 106}, potentially complicating the search for organic compounds including biosignatures with mass spectrometers such as the SUDA instrument onboard the upcoming Europa Clipper mission or a future Enceladus mission¹⁰¹. Using the LILBID setup to simulate the process of impact ionization of organic- and salt-rich ice grains in space, we showed that a wide variety of individual organic species could be detected by SUDA-type mass spectrometers although these samples can be analytically demanding. The presence of functional groups and the molecular structure and physico-chemical properties of the organics play a major role in the detectability of the organic species. The recorded mass spectra allowed us to establish general rules for the identification of organic species in a NaCl-rich matrix:

- protonated and deprotonated molecular peaks are usually suppressed because of “salt-in” effects with increasing NaCl concentrations, as observed in both ion mode. Organic species can still be detected by the identification of molecular ions and sodiated and chlorinated adducts.

- carboxylic acids, due to their high acidity, have highly characteristic mass spectral signatures with signals of high intensity especially in anion mass spectra. They tend to form $[M-H]^-$ in the presence of water¹⁰⁷ and therefore are detectable by prominent deprotonated molecular peaks $[M-H]^-$ in anion mode even with high salt concentrations. In cation mode, they can be detected by highly prominent disodiated $[M-H+2Na]^+$ peaks.
- organic species bearing hydroxyl (OH) groups typically form abundant molecular anions, allowing a good detectability in anion mode. They are usually also well detected in cation mode owing to their sodiated adducts.
- organic species bearing amine (NH₂) groups tend to have a low response in anion mode and an intermediate response in cation mode. Other functional groups or other properties of the organic species may increase their sensitivity (e.g. amino acids have a high sensitivity in salt-rich ice grains with impact ionization mass spectrometry⁶⁷).
- highly acidic compounds are expected to be highly responsive in anion analysis. However, we believe that acidity alone cannot predict the sensitivity of anions, which is also influenced by other physicochemical factors such as the molecular structure, its polarity or the presence of functional groups.
- polysodiated complexes formed from the substitution of carboxylic or amidic protons by Na⁺ are expected for organic species containing hydroxyl and/or amine functional groups.
- organic fragments are expected to form from organic species having hydroxyl, amine and carboxylic groups by the cleavage of these groups. Typical fragments include for hydroxyl-bearing organics $[M-OH]^+$; for amine-bearing organics $[M-NH_2]^+$, $[NH_4]^+$, and $[CH_2NH_2]^+$; and, for carboxylic acids $[M-COOH]^-$ and $[M-$

OH]⁺. On the contrary, aromatic ring systems significantly inhibit fragmentation processes.

- the mass spectrometric signal of organics in anion mode is usually lower than that in cation mode (except for acidic species) and greatly depends on the organics' physicochemical properties.

Although these rules were established from investigations on a limited range of representative organic species, we believe that they are transferrable to different organic compounds having similar pH values and functional groups. Whereas we investigated rather “simple” samples composed of only one organic species in NaCl matrix, the targets of SUDA-type instruments are natural samples from icy moons likely to be mixtures of several compounds. On the one hand, the effects of inorganic content of the ice grains require more laboratory investigations focusing on the spectral signatures of different types of salts and other non-ice components of icy moons' surfaces. We currently also perform experiments with inorganic components expected to be found in the matrix of ice grains ejected from Europa or Enceladus, including sulfates ⁴⁶, sulfuric acid ^{43,44}, and magnesium salts. On the other hand, definitive identification of organic species can be complicated by potential interferences in complex mixtures. To resolve such ambiguities, comparison of isobaric masses can be performed with the high mass resolution of mass spectrometers to establish mass differences <1u as shown in Klenner et al. ⁶⁷. Besides, the rules established here can allow the identification of functional groups in a sample, if not the definitive identification of an organic species. The recorded LILBID mass spectra complement a comprehensive spectral reference library for impact ionization mass spectrometers onboard Europa Clipper and other ocean world missions ⁷⁷, which will undoubtedly help to resolve the ambiguities encountered with complex salt-rich ice matrices and allow a better characterization of icy moons' oceanic and surface composition in the next decades.

6 Supporting Information

Additional LILBID mass spectra for all organic species measured in pure water and NaCl-rich matrices; Lists of fragment peaks detected for each organic species in increasing NaCl matrices.

7 Acknowledgment

This work was conducted at Freie Universität Berlin and supported by the European Research Council (ERC) under the European Union's Horizon 2020 research and innovation program by the Consolidator Grant 724908 Habitat-OASIS.

8 Abbreviations

CDA, Cosmic Dust Analyzer; ENIA, Enceladus Ice Analyzer; ESI, electrospray ionization; LILBID, Laser Induced Liquid Beam Ion Desorption; MALDI, Matrix Assisted Laser Desorption Ionization; MS, mass spectrometry; NIMS, Near-Infrared Mapping Spectrometer; SUDA, SURface Dust Analyzer; TOF, time-of-flight.

References

- (1) Khurana, K. K.; Kivelson, M. G.; Stevenson, D. J.; Schubert, G.; Russell, C. T.; Walker, R. J.; Polansky, C. Induced Magnetic Fields as Evidence for Subsurface Oceans in Europa and Callisto. *Nature* **1998**, *395* (6704), 777–780. <https://doi.org/10.1038/27394>.
- (2) Kivelson, M. G.; Khurana, K. K.; Russell, C. T.; Volwerk, M.; Walker, R. J.; Zimmer, C. Galileo Magnetometer Measurements: A Stronger Case for a Subsurface Ocean at Europa. *Science* **2000**, *289* (5483), 1340–1343. <https://doi.org/10.1126/science.289.5483.1340>.

- (3) Hand, K. P.; Carlson, R. W.; Chyba, C. F. Energy, Chemical Disequilibrium, and Geological Constraints on Europa. *Astrobiology* **2007**, *7* (6), 1006–1022. <https://doi.org/10.1089/ast.2007.0156>.
- (4) Thomas, P. C.; Tajeddine, R.; Tiscareno, M. S.; Burns, J. A.; Joseph, J.; Lored, T. J.; Helfenstein, P.; Porco, C. Enceladus's Measured Physical Libration Requires a Global Subsurface Ocean. *Icarus* **2016**, *264*, 37–47. <https://doi.org/10.1016/j.icarus.2015.08.037>.
- (5) Chyba, C. Correction: Energy for Microbial Life on Europa. *Nature* **2000**, *406* (6794), 368–368. <https://doi.org/10.1038/35019159>.
- (6) Anderson, J. D.; Schubert, G.; Jacobson, R. A.; Lau, E. L.; Moore, W. B.; Sjogren, W. L. Europa's Differentiated Internal Structure: Inferences from Four Galileo Encounters. *Science* **1998**, *281* (5385), 2019–2022. <https://doi.org/10.1126/science.281.5385.2019>.
- (7) Zolotov, M. Y.; Shock, E. L. Composition and Stability of Salts on the Surface of Europa and Their Oceanic Origin. *J. Geophys. Res.* **2001**, *106* (E12), 32815–32827. <https://doi.org/10.1029/2000JE001413>.
- (8) Canup, R. M.; Ward, W. R. Formation of the Galilean Satellites: Conditions of Accretion. *The Astronomical Journal* **2002**, *124* (6), 3404–3423. <https://doi.org/10.1086/344684>.
- (9) Moore, W. B.; Hussmann, H.; Pappalardo, R. T.; McKinnon, W. B.; Khurana, K. Thermal evolution of Europa's silicate interior. In *Europa* (p. 369). University of Arizona Press. **2009**
- (10) Vance, S. D.; Hand, K. P.; Pappalardo, R. T. Geophysical Controls of Chemical Disequilibria in Europa. *Geophys. Res. Lett.* **2016**, *43* (10), 4871–4879. <https://doi.org/10.1002/2016GL068547>.
- (11) Russell, M. J.; Murray, A. E.; Hand, K. P. The Possible Emergence of Life and Differentiation of a Shallow Biosphere on Irradiated Icy Worlds: The Example of Europa. *Astrobiology* **2017**, *17* (12), 1265–1273. <https://doi.org/10.1089/ast.2016.1600>.
- (12) Postberg, F.; Kempf, S.; Schmidt, J.; Brilliantov, N.; Beinsen, A.; Abel, B.; Buck, U.; Srama, R. Sodium Salts in E-Ring Ice Grains from an Ocean below the Surface of Enceladus. *Nature* **2009**, *459* (7250), 1098–1101. <https://doi.org/10.1038/nature08046>.
- (13) Postberg, F.; Schmidt, J.; Hillier, J.; Kempf, S.; Srama, R. A Salt-Water Reservoir as the Source of a Compositionally Stratified Plume on Enceladus. *Nature* **2011**, *474* (7353), 620–622. <https://doi.org/10.1038/nature10175>.
- (14) Waite Jr, J. H.; Lewis, W. S.; Magee, B. A.; Lunine, J. I.; McKinnon, W. B.; Glein, C. R.; Mousis, O.; Young, D. T.; Brockwell, T.; Westlake, J.; Nguyen, M.-J.; Teolis, B. D.; Niemann, H. B.; McNutt Jr, R. L.; Perry, M.; Ip, W.-H. Liquid Water on Enceladus from Observations of Ammonia and 40Ar in the Plume. *Nature* **2009**, *460* (7254), 487–490. <https://doi.org/10.1038/nature08153>.
- (15) Postberg, F.; Khawaja, N.; Abel, B.; Choblet, G.; Glein, C. R.; Gudipati, M. S.; Henderson, B. L.; Hsu, H.-W.; Kempf, S.; Klenner, F.; Moragas-Klostermeyer, G.; Magee, B.; Nölle, L.; Perry, M.; Reviol, R.; Schmidt, J.; Srama, R.; Stolz, F.; Tobie, G.; Trieloff, M.; Waite, J. H. Macromolecular Organic Compounds from the Depths of Enceladus. *Nature* **2018**, *558* (7711), 564–568. <https://doi.org/10.1038/s41586-018-0246-4>.
- (16) Khawaja, N.; Postberg, F.; Hillier, J.; Klenner, F.; Kempf, S.; Nölle, L.; Reviol, R.; Zou, Z.; Srama, R. Low-Mass Nitrogen-, Oxygen-Bearing, and Aromatic Compounds in Enceladean Ice Grains. *Monthly Notices of the Royal Astronomical Society* **2019**, *489* (4), 5231–5243. <https://doi.org/10.1093/mnras/stz2280>.

- (17) Postberg, F.; Sekine, Y.; Klenner F.; Glein, C.; Zou Z.; Abel, B.; Furuya, K.; Hillier J.K.; Khawaja N.; Kempf, S.; Nölle L.; Saito, T.; Schmidt J.; Shibuya, T.; Srama, R; Tan, S. Detection of Phosphates Originating from Enceladus' Ocean. *Nature* **2022**, under review.
- (18) Hsu, H.-W.; Postberg, F.; Sekine, Y.; Shibuya, T.; Kempf, S.; Horányi, M.; Juhász, A.; Altobelli, N.; Suzuki, K.; Masaki, Y.; Kuwatani, T.; Tachibana, S.; Sirono, S.; Moragas-Klostermeyer, G.; Srama, R. Ongoing Hydrothermal Activities within Enceladus. *Nature* **2015**, *519* (7542), 207–210. <https://doi.org/10.1038/nature14262>.
- (19) Waite, J. H.; Glein, C. R.; Perryman, R. S.; Teolis, B. D.; Magee, B. A.; Miller, G.; Grimes, J.; Perry, M. E.; Miller, K. E.; Bouquet, A.; Lunine, J. I.; Brockwell, T.; Bolton, S. J. Cassini Finds Molecular Hydrogen in the Enceladus Plume: Evidence for Hydrothermal Processes. *Science* **2017**, *356* (6334), 155–159. <https://doi.org/10.1126/science.aai8703>.
- (20) Porco, C. C.; Helfenstein, P.; Thomas, P. C.; Ingersoll, A. P.; Wisdom, J.; West, R.; Neukum, G.; Denk, T.; Wagner, R.; Roatsch, T.; Kieffer, S.; Turtle, E.; McEwen, A.; Johnson, T. V.; Rathbun, J.; Veverka, J.; Wilson, D.; Perry, J.; Spitale, J.; Brahic, A.; Burns, J. A.; DelGenio, A. D.; Dones, L.; Murray, C. D.; Squyres, S. Cassini Observes the Active South Pole of Enceladus. *Science* **2006**, *311* (5766), 1393–1401. <https://doi.org/10.1126/science.1123013>.
- (21) Hansen, C. J.; Esposito, L.; Stewart, A. I. F.; Colwell, J.; Hendrix, A.; Pryor, W.; Shemansky, D.; West, R. Enceladus' Water Vapor Plume. *Science* **2006**, *311* (5766), 1422–1425. <https://doi.org/10.1126/science.1121254>.
- (22) Figueredo, P. H.; Greeley, R. Resurfacing History of Europa from Pole-to-Pole Geological Mapping. *Icarus* **2004**, *167* (2), 287–312. <https://doi.org/10.1016/j.icarus.2003.09.016>.
- (23) V. Krivov, A.; Sremčević, M.; Spahn, F.; Dikarev, V. V.; Kholshchevnikov, K. V. Impact-Generated Dust Clouds around Planetary Satellites: Spherically Symmetric Case. *Planetary and Space Science* **2003**, *51* (3), 251–269. [https://doi.org/10.1016/S0032-0633\(02\)00147-2](https://doi.org/10.1016/S0032-0633(02)00147-2).
- (24) Miljković, K.; Hillier, J. K.; Mason, N. J.; Zarnecki, J. C. Models of Dust around Europa and Ganymede. *Planetary and Space Science* **2012**, *70* (1), 20–27. <https://doi.org/10.1016/j.pss.2012.06.006>.
- (25) Johnson, R. E.; Sundqvist, B. U. R. Sputtering and Detection of Large Organic Molecules from Europa. *Icarus* **2018**, *309*, 338–344. <https://doi.org/10.1016/j.icarus.2018.01.027>.
- (26) Roth, L.; Saur, J.; Retherford, K. D.; Strobel, D. F.; Feldman, P. D.; McGrath, M. A.; Nimmo, F. Transient Water Vapor at Europa's South Pole. *Science* **2014**, *343* (6167), 171–174. <https://doi.org/10.1126/science.1247051>.
- (27) Sparks, W. B.; Hand, K. P.; McGrath, M. A.; Bergeron, E.; Cracraft, M.; Deustua, S. E. PROBING FOR EVIDENCE OF PLUMES ON EUROPA WITH *HST* /STIS. *ApJ* **2016**, *829* (2), 121. <https://doi.org/10.3847/0004-637X/829/2/121>.
- (28) Jia, X.; Kivelson, M. G.; Khurana, K. K.; Kurth, W. S. Evidence of a Plume on Europa from Galileo Magnetic and Plasma Wave Signatures. *Nat Astron* **2018**, *2* (6), 459–464. <https://doi.org/10.1038/s41550-018-0450-z>.
- (29) Paganini, L.; Villanueva, G. L.; Roth, L.; Mandell, A. M.; Hurford, T. A.; Retherford, K. D.; Mumma, M. J. A Measurement of Water Vapour amid a Largely Quiescent Environment on Europa. *Nat Astron* **2020**, *4* (3), 266–272. <https://doi.org/10.1038/s41550-019-0933-6>.

- (30) Huber, C.; Eisenreich, W.; Hecht, S.; Wächtershäuser, G. A Possible Primordial Peptide Cycle. *Science* **2003**, *301* (5635), 938–940. <https://doi.org/10.1126/science.1086501>.
- (31) Proskurowski, G.; Lilley, M. D.; Seewald, J. S.; Früh-Green, G. L.; Olson, E. J.; Lupton, J. E.; Sylva, S. P.; Kelley, D. S. Abiogenic Hydrocarbon Production at Lost City Hydrothermal Field. *Science* **2008**, *319* (5863), 604–607. <https://doi.org/10.1126/science.1151194>.
- (32) Novikov, Y.; Copley, S. D. Reactivity Landscape of Pyruvate under Simulated Hydrothermal Vent Conditions. *Proc. Natl. Acad. Sci. U.S.A.* **2013**, *110* (33), 13283–13288. <https://doi.org/10.1073/pnas.1304923110>.
- (33) Porco, C. C.; Dones, L.; Mitchell, C. Could It Be Snowing Microbes on Enceladus? Assessing Conditions in Its Plume and Implications for Future Missions. *Astrobiology* **2017**, *17* (9), 876–901. <https://doi.org/10.1089/ast.2017.1665>.
- (34) Srama, R.; Woiwode, W.; Postberg, F.; Armes, S. P.; Fujii, S.; Dupin, D.; Ormond-Prout, J.; Sternovsky, Z.; Kempf, S.; Moragas-Klostermeyer, G.; Mockler, A.; Grün, E. Mass Spectrometry of Hyper-Velocity Impacts of Organic Micrograins: MS Study of Hyper-Velocity Impacts of Organic Micrograins. *Rapid Commun. Mass Spectrom.* **2009**, *23* (24), 3895–3906. <https://doi.org/10.1002/rcm.4318>.
- (35) Postberg, F.; Clark, R. N.; Hansen, C. J.; Coates, A. J.; Dalle Ore, C. M.; Scipioni, F.; Hedman, M.; Waite, H. J. Plume and surface composition of Enceladus. *Enceladus and the icy moons of Saturn*, 2018, 129-162.
- (36) Glein, C. R.; Postberg, F.; Vance, S. D. The geochemistry of Enceladus: composition and controls. *Enceladus and the icy moons of Saturn*, 2018, 39.
- (37) Howell, S. M.; Pappalardo, R. T. NASA's Europa Clipper—a Mission to a Potentially Habitable Ocean World. *Nat Commun* **2020**, *11* (1), 1311. <https://doi.org/10.1038/s41467-020-15160-9>.
- (38) Kempf, S.; Altobelli, N.; Briois, C.; Grün, E.; Horanyi, M.; Postberg, F.; Schmidt, J.; Srama, R.; Sternovsky, Z.; Tobie, G.; Zolotov, M. SUDA: a dust mass spectrometer for compositional surface mapping for a mission to Europa. In International Workshop on Instrumentation for Planetary Missions (Vol. 3, p. 7) **2014**.
- (39) Goode, W.; Kempf, S.; Schmidt, J. Detecting the Surface Composition of Geological Features on Europa and Ganymede Using a Surface Dust Analyzer. *Planetary and Space Science* **2021**, *208*, 105343. <https://doi.org/10.1016/j.pss.2021.105343>.
- (40) Zeng, Y.; Jansen, M. F. Ocean Circulation on Enceladus with a High- versus Low-Salinity Ocean. *Planet. Sci. J.* **2021**, *2* (4), 151. <https://doi.org/10.3847/PSJ/ac1114>.
- (41) Kang, W.; Mittal, T.; Bire, S.; Campin, J.-M.; Marshall, J. How Does Salinity Shape Ocean Circulation and Ice Geometry on Enceladus and Other Icy Satellites? *Sci. Adv.* **2022**, *8* (29), eabm4665. <https://doi.org/10.1126/sciadv.abm4665>.
- (42) Hand, K.; Chyba, C. Empirical Constraints on the Salinity of the European Ocean and Implications for a Thin Ice Shell. *Icarus* **2007**, *189* (2), 424–438. <https://doi.org/10.1016/j.icarus.2007.02.002>.
- (43) Carlson, R. W.; Johnson, R. E.; Anderson, M. S. Sulfuric Acid on Europa and the Radiolytic Sulfur Cycle. *Science* **1999**, *286* (5437), 97–99. <https://doi.org/10.1126/science.286.5437.97>.

- (44) Carlson, R. W.; Anderson, M. S.; Johnson, R. E.; Schulman, M. B.; Yavrouian, A. H. Sulfuric Acid Production on Europa: The Radiolysis of Sulfur in Water Ice. *Icarus* **2002**, *157* (2), 456–463. <https://doi.org/10.1006/icar.2002.6858>.
- (45) Carlson, R. W.; Anderson, M. S.; Mehlman, R.; Johnson, R. E. Distribution of Hydrate on Europa: Further Evidence for Sulfuric Acid Hydrate. *Icarus* **2005**, *177* (2), 461–471. <https://doi.org/10.1016/j.icarus.2005.03.026>.
- (46) Brown, M. E.; Hand, K. P. SALTS AND RADIATION PRODUCTS ON THE SURFACE OF EUROPA. *AJ* **2013**, *145* (4), 110. <https://doi.org/10.1088/0004-6256/145/4/110>.
- (47) Fischer, P. D.; Brown, M. E.; Hand, K. P. SPATIALLY RESOLVED SPECTROSCOPY OF EUROPA: THE DISTINCT SPECTRUM OF LARGE-SCALE CHAOS. *AJ* **2015**, *150* (5), 164. <https://doi.org/10.1088/0004-6256/150/5/164>.
- (48) McCord, T. B.; Hansen, G. B.; Fanale, F. P.; Carlson, R. W.; Matson, D. L.; Johnson, T. V.; Smythe, W. D.; Crowley, J. K.; Martin, P. D.; Ocampo, A.; Hibbitts, C. A.; Granahan, J. C.; the NIMS Team. Salts on Europa's Surface Detected by Galileo's Near Infrared Mapping Spectrometer. *Science* **1998**, *280* (5367), 1242–1245. <https://doi.org/10.1126/science.280.5367.1242>.
- (49) Dalton, J. B. Linear Mixture Modeling of Europa's Non-Ice Material Based on Cryogenic Laboratory Spectroscopy. *Geophys. Res. Lett.* **2007**, *34* (21), L21205. <https://doi.org/10.1029/2007GL031497>.
- (50) Dalton, J. B.; Shirley, J. H.; Kamp, L. W. Europa's Icy Bright Plains and Dark Linea: Exogenic and Endogenic Contributions to Composition and Surface Properties: EUROPA-ICY BRIGHT PLAINS AND DARK LINEA. *J. Geophys. Res.* **2012**, *117* (E3), n/a-n/a. <https://doi.org/10.1029/2011JE003909>.
- (51) Dalton, J. B.; Cassidy, T.; Paranicas, C.; Shirley, J. H.; Prockter, L. M.; Kamp, L. W. Exogenic Controls on Sulfuric Acid Hydrate Production at the Surface of Europa. *Planetary and Space Science* **2013**, *77*, 45–63. <https://doi.org/10.1016/j.pss.2012.05.013>.
- (52) Ligier, N.; Poulet, F.; Carter, J.; Brunetto, R.; Gourgéot, F. VLT/SINFONI OBSERVATIONS OF EUROPA: NEW INSIGHTS INTO THE SURFACE COMPOSITION. *The Astronomical Journal* **2016**, *151* (6), 163. <https://doi.org/10.3847/0004-6256/151/6/163>.
- (53) O'Brien, D. A Melt-through Model for Chaos Formation on Europa. *Icarus* **2002**, *156* (1), 152–161. <https://doi.org/10.1006/icar.2001.6777>.
- (54) Sotin, C.; Head, J. W.; Tobie, G. Europa: Tidal Heating of Upwelling Thermal Plumes and the Origin of Lenticulae and Chaos Melting: TIDAL HEATING OF EUROPEAN PLUMES. *Geophys. Res. Lett.* **2002**, *29* (8), 74-1-74-4. <https://doi.org/10.1029/2001GL013844>.
- (55) Trumbo, S. K.; Brown, M. E.; Hand, K. P. Sodium Chloride on the Surface of Europa. *Sci. Adv.* **2019**, *5* (6), eaaw7123. <https://doi.org/10.1126/sciadv.aaw7123>.
- (56) Trumbo, S. K.; Becker, T. M.; Brown, M. E.; Denman, W. T. P.; Molyneux, P.; Hendrix, A.; Retherford, K. D.; Roth, L.; Alday, J. A New UV Spectral Feature on Europa: Confirmation of NaCl in Leading-Hemisphere Chaos Terrain. *Planet. Sci. J.* **2022**, *3* (2), 27. <https://doi.org/10.3847/PSJ/ac4580>.

(57) Brown, M. E.; Denman, W. T. P.; Trumbo, S. K. The Mid-UV Spectrum of Irradiated NaCl at Europa-like Conditions. *Planet. Sci. J.* **2022**, 3 (2), 28.

<https://doi.org/10.3847/PSJ/ac457f>.

(58) Kargel, J. S.; Kaye, J. Z.; Head, J. W.; Marion, G. M.; Sassen, R.; Crowley, J. K.; Ballesteros, O. P.; Grant, S. A.; Hogenboom, D. L. Europa's Crust and Ocean: Origin, Composition, and the Prospects for Life. *Icarus* **2000**, 148 (1), 226–265.

<https://doi.org/10.1006/icar.2000.6471>.

(59) Hand, K. P.; Phillips, C. B.; Murray, A.; Garvin, J. B.; Maize, E. H.; Gibbs, R. G.; Reeves, G.; Martin, A. M. S.; Tan-Wang, G. H.; Krajewski, J.; Hurst, K.; Crum, R.; Kennedy, B. A.; McElrath, T. P.; Gallon, J. C.; Sabahi, D.; Thurman, S. W.; Goldstein, B.; Estabrook, P.; Lee, S. W.; Dooley, J. A.; Brinckerhoff, W. B.; Edgett, K. S.; German, C. R.; Hoehler, T. M.; Hörst, S. M.; Lunine, J. I.; Paranicas, C.; Neelson, K.; Smith, D. E.; Templeton, A. S.; Russell, M. J.; Schmidt, B.; Christner, B.; Ehlmann, B.; Hayes, A.; Rhoden, A.; Willis, P.; Yingst, R. A.; Craft, K.; Cameron, M. E.; Nordheim, T.; Pitesky, J.; Scully, J.; Hofgartner, J.; Sell, S. W.; Barltrop, K. J.; Izraelevitz, J.; Brandon, E. J.; Seong, J.; Jones, J.-P.; Pasalic, J.; Billings, K. J.; Ruiz, J. P.; Bugga, R. V.; Graham, D.; Arenas, L. A.; Takeyama, D.; Drummond, M.; Aghazarian, H.; Andersen, A. J.; Andersen, K. B.; Anderson, E. W.; Babuscia, A.; Backes, P. G.; Bailey, E. S.; Balentine, D.; Ballard, C. G.; Berisford, D. F.; Bhandari, P.; Blackwood, K.; Bolotin, G. S.; Bovre, E. A.; Bowkett, J.; Boykins, K. T.; Bramble, M. S.; Brice, T. M.; Briggs, P.; Brinkman, A. P.; Brooks, S. M.; Buffington, B. B.; Burns, B.; Cable, M. L.; Campagnola, S.; Cangahuala, L. A.; Carr, G. A.; Casani, J. R.; Chahat, N. E.; Chamberlain-Simon, B. K.; Cheng, Y.; Chien, S. A.; Cook, B. T.; Cooper, M.; DiNicola, M.; Clement, B.; Dean, Z.; Cullimore, E. A.; Curtis, A. G.; Croix, J.-P. de la; Pasquale, P. D.; Dodd, E. M.; Dubord, L. A.; Edlund, J. A.; Ellyin, R.; Emanuel, B.; Foster, J. T.; Ganino, A. J.; Garner, G. J.; Gibson, M. T.; Gildner, M.; Glazebrook, K. J.; Greco, M. E.; Green, W. M.; Hatch, S. J.; Hetzel, M. M.; Hoey, W. A.; Hofmann, A. E.; Ionasescu, R.; Jain, A.; Jasper, J. D.; Johannesen, J. R.; Johnson, G. K.; Jun, I.; Katake, A. B.; Kim-Castet, S. Y.; Kim, D. I.; Kim, W.; Klonicki, E. F.; Kobeissi, B.; Kobie, B. D.; Kochocki, J.; Kokorowski, M.; Kosberg, J. A.; Kriechbaum, K.; Kulkarni, T. P.; Lam, R. L.; Landau, D. F.; Lattimore, M. A.; Laubach, S. L.; Lawler, C. R.; Lim, G.; Lin, J. Y.; Litwin, T. E.; Lo, M. W.; Logan, C. A.; Maghasoudi, E.; Mandrake, L.; Marchetti, Y.; Marteau, E.; Maxwell, K. A.; Namee, J. B. M.; Mcintyre, O.; Meacham, M.; Melko, J. P.; Mueller, J.; Muliere, D. A.; Mysore, A.; Nash, J.; Ono, H.; Parker, J. M.; Perkins, R. C.; Petropoulos, A. E.; Gaut, A.; Gomez, M. Y. P.; Casillas, R. P.; Preudhomme, M.; Pyrzak, G.; Rapinchuk, J.; Ratliff, J. M.; Ray, T. L.; Roberts, E. T.; Roffo, K.; Roth, D. C.; Russino, J. A.; Schmidt, T. M.; Schoppers, M. J.; Senent, J. S.; Serricchio, F.; Sheldon, D. J.; Shiraishi, L. R.; Shirvanian, J.; Siegel, K. J.; Singh, G.; Sirota, A. R.; Skulsky, E. D.; Stehly, J. S.; Strange, N. J.; Stevens, S. U.; Sunada, E. T.; Tepsuporn, S. P.; Tosi, L. P. C.; Trawny, N.; Uchenik, I.; Verma, V.; Volpe, R. A.; Wagner, C. T.; Wang, D.; Willson, R. G.; Wolff, J. L.; Wong, A. T.; Zimmer, A. K.; Sukhatme, K. G.; Bago, K. A.; Chen, Y.; Deardorff, A. M.; Kuch, R. S.; Lim, C.; Syvertson, M. L.; Arakaki, G. A.; Avila, A.; DeBruin, K. J.; Frick, A.; Harris, J. R.; Heverly, M. C.; Kawata, J. M.; Kim, S.-K.; Kipp, D. M.; Murphy, J.; Smith, M. W.; Spaulding, M. D.; Thakker, R.; Warner, N. Z.; Yahnker, C. R.; Young, M. E.; Magner, T.; Adams, D.; Bedini, P.; Mehr, L.; Sheldon, C.; Vernon, S.; Bailey, V.; Briere, M.; Butler, M.; Davis, A.; Ensor, S.; Gannon, M.; Haapala-Chalk, A.; Hartka, T.; Holdridge, M.; Hong, A.; Hunt, J.; Iskow, J.; Kahler, F.; Murray, K.; Napolillo, D.; Norkus, M.; Pfisterer, R.; Porter, J.; Roth, D.; Schwartz, P.; Wolfarth, L.; Cardiff, E. H.; Davis, A.; Grob, E. W.; Adam, J. R.; Betts, E.; Norwood, J.; Heller, M. M.; Voskuilen, T.; Sakievich, P.; Gray, L.; Hansen, D. J.; Irick, K. W.; Hewson, J. C.; Lamb, J.; Stacy, S. C.; Brotherton, C. M.; Tappan, A. S.; Benally, D.;

- Thigpen, H.; Ortiz, E.; Sandoval, D.; Ison, A. M.; Warren, M.; Stromberg, P. G.; Thelen, P. M.; Blasy, B.; Nandy, P.; Haddad, A. W.; Trujillo, L. B.; Wiseley, T. H.; Bell, S. A.; Teske, N. P.; Post, C.; Torres-Castro, L.; Grosso, C.; Wasiolek, M. Science Goals and Mission Architecture of the Europa Lander Mission Concept. *Planet. Sci. J.* **2022**, 3 (1), 22. <https://doi.org/10.3847/PSJ/ac4493>.
- (60) Belousov, A.; Miller, M.; Continetti, R.; Madzunkov, S.; Simcic, J.; Nikolic, D.; Maiwald, F.; Waller, S.; Malaska, M.; Cable, M. Sampling Accelerated Micron Scale Ice Particles with a Quadrupole Ion Trap Mass Spectrometer. *J. Am. Soc. Mass Spectrom.* **2021**, 32 (5), 1162–1168. <https://doi.org/10.1021/jasms.0c00442>.
- (61) New, J. S.; Kazemi, B.; Spathis, V.; Price, M. C.; Mathies, R. A.; Butterworth, A. L. Quantitative Evaluation of the Feasibility of Sampling the Ice Plumes at Enceladus for Biomarkers of Extraterrestrial Life. *Proc. Natl. Acad. Sci. U.S.A.* **2021**, 118 (37), e2106197118. <https://doi.org/10.1073/pnas.2106197118>.
- (62) Kleinekofort, W.; Avdiev, J.; Brutschy, B. A New Method of Laser Desorption Mass Spectrometry for the Study of Biological Macromolecules. *International Journal of Mass Spectrometry and Ion Processes* **1996**, 152 (2–3), 135–142. [https://doi.org/10.1016/0168-1176\(95\)04330-6](https://doi.org/10.1016/0168-1176(95)04330-6).
- (63) Kleinekofort, W.; Pfenninger, A.; Plomer, T.; Griesinger, C.; Brutschy, B. Observation of Noncovalent Complexes Using Laser-Induced Liquid Beam Ionization/Desorption. *International Journal of Mass Spectrometry and Ion Processes* **1996**, 156 (3), 195–202. [https://doi.org/10.1016/S0168-1176\(96\)04507-7](https://doi.org/10.1016/S0168-1176(96)04507-7).
- (64) Klenner, F.; Postberg, F.; Hillier, J.; Khawaja, N.; Reviol, R.; Srama, R.; Abel, B.; Stolz, F.; Kempf, S. Analogue Spectra for Impact Ionization Mass Spectra of Water Ice Grains Obtained at Different Impact Speeds in Space. *Rapid Commun Mass Spectrom* **2019**, 33 (22), 1751–1760. <https://doi.org/10.1002/rcm.8518>.
- (65) Khawaja, N.; Hillier, J.; Klenner, F.; Nölle, L.; Zou, Z.; Napoleoni, M.; Reviol, R.; Postberg, F. Complementary mass spectral analysis of isomeric O-bearing organic compounds and fragmentation differences through analogue techniques for spaceborne mass spectrometers. *Planet. Sci. J.*, **2022** accepted
- (66) Klenner, F.; Postberg, F.; Hillier, J.; Khawaja, N.; Reviol, R.; Stolz, F.; Cable, M. L.; Abel, B.; Nölle, L. Analog Experiments for the Identification of Trace Biosignatures in Ice Grains from Extraterrestrial Ocean Worlds. *Astrobiology* **2020a**, 20 (2), 179–189. <https://doi.org/10.1089/ast.2019.2065>.
- (67) Klenner, F.; Postberg, F.; Hillier, J.; Khawaja, N.; Cable, M. L.; Abel, B.; Kempf, S.; Glein, C. R.; Lunine, J. I.; Hodyss, R.; Reviol, R.; Stolz, F. Discriminating Abiotic and Biotic Fingerprints of Amino Acids and Fatty Acids in Ice Grains Relevant to Ocean Worlds. *Astrobiology* **2020b**, 20 (10), 1168–1184. <https://doi.org/10.1089/ast.2019.2188>.
- (68) Srama, R.; Postberg, F.; Henkel, H.; Klopfer, T.; Li, Y.; Simolka, J.; Bugiel, S.; Kempf, S.; Hillier, J.; Khawaja, N.; Triefoff, M.; Abel, B.; Moragas-Klostermeyer, G.; Strack, H.; Schmidt, J.; Soja, R.; Sternovsky, Z.; Spohn, T. Enceladus Icy Jet Analyzer (ENIJA): Search for life with a high resolution TOF-MS for in situ characterization of high dust density regions. *Eur. Planet. Sci. Congr.* **2015** 10:EPSC2015-769.
- (69) Dannenmann, M.; Klenner, F.; Bönigk, J.; Pavlista, M.; Napoleoni, M.; Hillier, J.; Khawaja, N.; Olsson-Francis, K.; Cable, M. L.; Malaska, M. J.; Abel, B.; Postberg, F. Toward Detecting Biosignatures of DNA, Lipids, and Metabolic Intermediates from Bacteria

- in Ice Grains Emitted by Enceladus and Europa. *Astrobiology* **2023**, *23* (1), 60–75.
<https://doi.org/10.1089/ast.2022.0063>.
- (70) Annesley, T. M. Ion Suppression in Mass Spectrometry. *Clinical Chemistry* **2003**, *49* (7), 1041–1044. <https://doi.org/10.1373/49.7.1041>.
- (71) Piwowar, A. M.; Lockyer, N. P.; Vickerman, J. C. Salt Effects on Ion Formation in Desorption Mass Spectrometry: An Investigation into the Role of Alkali Chlorides on Peak Suppression in Time-of-Flight-Secondary Ion Mass Spectrometry. *Anal. Chem.* **2009**, *81* (3), 1040–1048. <https://doi.org/10.1021/ac8020888>.
- (72) Stern, R.; Jedrzejewski, M. J. Carbohydrate Polymers at the Center of Life's Origins: The Importance of Molecular Processivity. *Chem. Rev.* **2008**, *108* (12), 5061–5085. <https://doi.org/10.1021/cr078240l>.
- (73) Furukawa, Y.; Chikaraishi, Y.; Ohkouchi, N.; Ogawa, N. O.; Glavin, D. P.; Dworkin, J. P.; Abe, C.; Nakamura, T. Extraterrestrial Ribose and Other Sugars in Primitive Meteorites. *Proc. Natl. Acad. Sci. U.S.A.* **2019**, *116* (49), 24440–24445. <https://doi.org/10.1073/pnas.1907169116>.
- (74) Rodriguez, L. E.; House, C. H.; Smith, K. E.; Roberts, M. R.; Callahan, M. P. Nitrogen Heterocycles Form Peptide Nucleic Acid Precursors in Complex Prebiotic Mixtures. *Sci Rep* **2019**, *9* (1), 9281. <https://doi.org/10.1038/s41598-019-45310-z>.
- (75) Charvat, A.; Abel, B. How to Make Big Molecules Fly out of Liquid Water: Applications, Features and Physics of Laser Assisted Liquid Phase Dispersion Mass Spectrometry. *Phys. Chem. Chem. Phys.* **2007**, *9* (26), 3335. <https://doi.org/10.1039/b615114k>.
- (76) Wiederschein, F.; Vöhringer-Martinez, E.; Beinsen, A.; Postberg, F.; Schmidt, J.; Srama, R.; Stolz, F.; Grubmüller, H.; Abel, B. Charge Separation and Isolation in Strong Water Droplet Impacts. *Phys. Chem. Chem. Phys.* **2015**, *17* (10), 6858–6864. <https://doi.org/10.1039/C4CP05618C>.
- (77) Klenner, F.; Umair, M.; Walter, S. H. G.; Khawaja, N.; Hillier, J.; Nölle, L.; Zou, Z.; Napoleoni, M.; Sanderink, A.; Zuschneid, W.; Abel, B.; Postberg, F. Developing a Laser Induced Liquid Beam Ion Desorption Spectral Database as Reference for Spaceborne Mass Spectrometers. *Earth and Space Science* **2022**, *9* (9). <https://doi.org/10.1029/2022EA002313>.
- (78) Mädler, S.; Barylyuk, K.; Boeri Erba, E.; Nieckarz, R. J.; Zenobi, R. Compelling Advantages of Negative Ion Mode Detection in High-Mass MALDI-MS for Homomeric Protein Complexes. *J. Am. Soc. Mass Spectrom.* **2012**, *23* (2), 213–224. <https://doi.org/10.1007/s13361-011-0274-x>.
- (79) Dashtiev, M.; Wäfler, E.; Röhling, U.; Gorshkov, M.; Hillenkamp, F.; Zenobi, R. Positive and Negative Analyte Ion Yield in Matrix-Assisted Laser Desorption/Ionization. *International Journal of Mass Spectrometry* **2007**, *268* (2–3), 122–130. <https://doi.org/10.1016/j.ijms.2007.07.001>.
- (80) Cech, N. B.; Enke, C. G. Practical Implications of Some Recent Studies in Electrospray Ionization Fundamentals. *Mass Spectrom. Rev.* **2001**, *20* (6), 362–387. <https://doi.org/10.1002/mas.10008>.

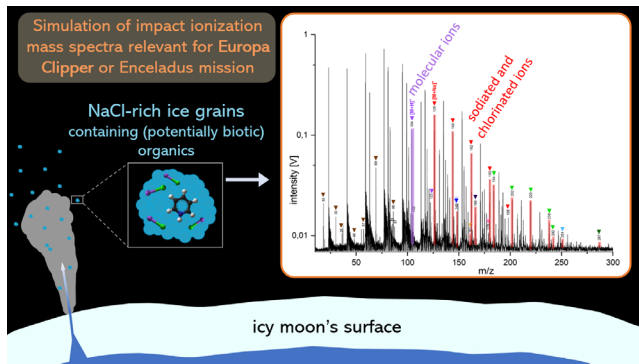
- (81) Oss, M.; Kruve, A.; Herodes, K.; Leito, I. Electrospray Ionization Efficiency Scale of Organic Compounds. *Anal. Chem.* **2010**, *82* (7), 2865–2872. <https://doi.org/10.1021/ac902856t>.
- (82) Hillenkamp, F.; Peter-Katalinic, J. *MALDI MS: A Practical Guide to Instrumentation, Methods and Applications.*, John Wiley&Sons.; 2013.
- (83) Kruve, A.; Kaupmees, K.; Liigand, J.; Leito, I. Negative Electrospray Ionization via Deprotonation: Predicting the Ionization Efficiency. *Anal. Chem.* **2014**, *86* (10), 4822–4830. <https://doi.org/10.1021/ac404066v>.
- (84) Liigand, J.; Laaniste, A.; Kruve, A. PH Effects on Electrospray Ionization Efficiency. *J. Am. Soc. Mass Spectrom.* **2017**, *28* (3), 461–469. <https://doi.org/10.1007/s13361-016-1563-1>.
- (85) Ferrer, I.; Zweigenbaum, J. A.; Thurman, E. M. Analytical Methodologies for the Detection of Sucralose in Water. *Anal. Chem.* **2013**, *85* (20), 9581–9587. <https://doi.org/10.1021/ac4016984>.
- (86) Sales, P.; de Souza, K.; Bezerra, A.; Ojala, S.; de Oliveira, S.; dos Santos, P.; Bara, M. T. How Sodiation Influences the Sucralose Behavior under Electrospray Ionization Mass Spectrometry. *Braz J Anal Chem* **2022**, *9* (36). <https://doi.org/10.30744/brjac.2179-3425.TN-99-2021>.
- (87) Newton, K. A.; McLuckey, S. A. Generation and Manipulation of Sodium Cationized Peptides in the Gas Phase. *J. Am. Soc. Mass Spectrom.* **2004**, *15* (4), 607–615. <https://doi.org/10.1016/j.jasms.2003.12.014>.
- (88) Rodriguez, C. F.; Guo, X.; Shoeib, T.; Hopkinson, A. C.; Siu, K. W. M. Formation of $[M - n H + m Na]^{(m-n)+}$ and $[M - n H + m K]^{(m-n)+}$ Ions in Electrospray Mass Spectrometry of Peptides and Proteins. *J. Am. Soc. Mass Spectrom.* **2000**, *11* (11), 967–975. [https://doi.org/10.1016/S1044-0305\(00\)00162-8](https://doi.org/10.1016/S1044-0305(00)00162-8).
- (89) Grewal, R. N.; Aribi, H. E.; Smith, J. C.; Rodriguez, C. F.; Hopkinson, A. C.; Siu, K. W. M. Multiple Substitution of Protons by Sodium Ions in Sodiated Oligoglycines. *International Journal of Mass Spectrometry* **2002**, *219* (1), 89–99. [https://doi.org/10.1016/S1387-3806\(02\)00561-4](https://doi.org/10.1016/S1387-3806(02)00561-4).
- (90) Chang, W. C.; Huang, L. C. L.; Wang, Y.-S.; Peng, W.-P.; Chang, H. C.; Hsu, N. Y.; Yang, W. B.; Chen, C. H. Matrix-Assisted Laser Desorption/Ionization (MALDI) Mechanism Revisited. *Analytica Chimica Acta* **2007**, *582* (1), 1–9. <https://doi.org/10.1016/j.aca.2006.08.062>.
- (91) Boutegrabet, L.; Kanawati, B.; Gebefügi, I.; Peyron, D.; Cayot, P.; Gougeon, R. D.; Schmitt-Kopplin, P. Attachment of Chloride Anion to Sugars: Mechanistic Investigation and Discovery of a New Dopant for Efficient Sugar Ionization/Detection in Mass Spectrometers. *Chem. Eur. J.* **2012**, *18* (41), 13059–13067. <https://doi.org/10.1002/chem.201103788>.
- (92) Phungsai, P.; Kurisu, F.; Kasuga, I.; Furumai, H. Molecular Characterization of Low Molecular Weight Dissolved Organic Matter in Water Reclamation Processes Using Orbitrap Mass Spectrometry. *Water Research* **2016**, *100*, 526–536. <https://doi.org/10.1016/j.watres.2016.05.047>.
- (93) Tannenbaum, H. P.; Roberts, J. D.; Dougherty, R. C. Negative chemical ionization mass spectrometry. Chloride attachment spectra. *Analytical Chemistry* **1975**, *47*(1), 49-54.

- (94) Mora, M. F.; Kok, M. G. M.; Noell, A.; Willis, P. A. Detection of Biosignatures by Capillary Electrophoresis Mass Spectrometry in the Presence of Salts Relevant to Ocean Worlds Missions. *Astrobiology* **2022**, *22* (8), 914–925. <https://doi.org/10.1089/ast.2021.0091>.
- (95) Constantopoulos, T. L.; Jackson, G. S.; Enke, C. G. Effects of Salt Concentration on Analyte Response Using Electrospray Ionization Mass Spectrometry. *J. Am. Soc. Mass Spectrom.* **1999**, *10* (7), 625–634. [https://doi.org/10.1016/S1044-0305\(99\)00031-8](https://doi.org/10.1016/S1044-0305(99)00031-8).
- (96) Pan, P.; McLuckey, S. A. The Effect of Small Cations on the Positive Electrospray Responses of Proteins at Low PH. *Anal. Chem.* **2003**, *75* (20), 5468–5474. <https://doi.org/10.1021/ac034344u>.
- (97) Postberg, F.; Kempf, S.; Hillier, J. K.; Srama, R.; Green, S. F.; McBride, N.; Grün, E. The E-Ring in the Vicinity of Enceladus. *Icarus* **2008**, *193* (2), 438–454. <https://doi.org/10.1016/j.icarus.2007.09.001>.
- (98) Furey, A.; Moriarty, M.; Bane, V.; Kinsella, B.; Lehane, M. Ion Suppression; A Critical Review on Causes, Evaluation, Prevention and Applications. *Talanta* **2013**, *115*, 104–122. <https://doi.org/10.1016/j.talanta.2013.03.048>.
- (99) Hand, K. P.; Chyba, C. F.; Priscu, J. C.; Carlson, R. W.; Neelson, K. H. Astrobiology and the potential for life on Europa. *Europa* **2009**, 589-629.
- (100) Kereszturi, A.; Keszthelyi, Z. Astrobiological implications of chaos terrains on Europa to help targeting future missions. *Planetary and Space Science* **2013**, *77*, 74-90. <https://doi.org/10.1016/j.pss.2012.08.028>
- (101) Reh, K.; Spilker, L.; Lunine, J. I.; Waite, J. H.; Cable, M. L.; Postberg, F.; Clark, K. Enceladus Life Finder: The search for life in a habitable moon. *IEEE Aerospace Conference* **2016**, (pp. 1-8).
- (102) Mitri, G.; Postberg, F.; Soderblom, J. M.; Wurz, P.; Tortora, P.; Abel, B.; Barnes, J. W.; Berga, M.; Carrasco, N.; Coustenis, A.; Paul de Vera, J. P.; D’Ottavio, A.; Ferri, F.; Hayes, A. G.; Hayne, P. O.; Hillier, J. K.; Kempf, S.; Lebreton, J.-P.; Lorenz, R. D.; Martelli, A.; Orosei, R.; Petropoulos, A. E.; Reh, K.; Schmidt, J.; Sotin, C.; Srama, R.; Tobie, G.; Vorburger, A.; Vuitton, V.; Wong, A.; Zannoni, M. Explorer of Enceladus and Titan (E2T): Investigating Ocean Worlds’ Evolution and Habitability in the Solar System. *Planetary and Space Science* **2018**, *155*, 73–90. <https://doi.org/10.1016/j.pss.2017.11.001>.
- (103) Lusci, G.; Pivetta, T.; Carucci, C.; Parsons, D. F.; Salis, A.; Monduzzi, M. BSA Fragmentation Specifically Induced by Added Electrolytes: An Electrospray Ionization Mass Spectrometry Investigation. *Colloids and Surfaces B: Biointerfaces* **2022**, *218*, 112726. <https://doi.org/10.1016/j.colsurfb.2022.112726>.
- (104) Shi, T.; Zhao, J.; Shek, P. I.; Hopkinson, A. C.; Siu, K. M. Carbonate, carbamate, urea, and guanidine as model species for functional groups in biological molecules A combined density functional theory and mass spectrometry examination of polysodiation and gas-phase dissociation. *Canadian journal of chemistry* **2005**, *83*(11), 1941-1952.
- (105) Jaramillo-Botero, A.; Cable, M. L.; Hofmann, A. E.; Malaska, M.; Hodyss, R.; Lunine, J. Understanding Hypervelocity Sampling of Biosignatures in Space Missions. *Astrobiology* **2021**, *21* (4), 421–442. <https://doi.org/10.1089/ast.2020.2301>.
- (106) Hand, K. P.; Carlson, R. W. Europa’s Surface Color Suggests an Ocean Rich with Sodium Chloride: Sodium Chloride on Europa’s Surface. *Geophys. Res. Lett.* **2015**, *42* (9), 3174–3178. <https://doi.org/10.1002/2015GL063559>.

(107) Henriksen, T.; Juhler, R. K.; Svensmark, B.; Cech, N. B. The Relative Influences of Acidity and Polarity on Responsiveness of Small Organic Molecules to Analysis with Negative Ion Electrospray Ionization Mass Spectrometry (ESI-MS). *J. Am. Soc. Mass Spectrom.* **2005**, *16* (4), 446–455. <https://doi.org/10.1016/j.jasms.2004.11.021>.

For TOC only

Table of Contents (TOC) graphic



All parts of the TOC graphic are entirely original, unpublished, and created by the first author.